

# Process-based modelling of the methane balance in periglacial landscapes (JSBACH-methane)

S. Kaiser<sup>1</sup>, M. Göckede<sup>1</sup>, K. Castro-Morales<sup>1</sup>, C. Knoblauch<sup>2</sup>, A. Ekici<sup>1,3</sup>,  
T. Kleinen<sup>4</sup>, S. Zubrzycki<sup>2</sup>, T. Sachs<sup>5</sup>, C. Wille<sup>2</sup>, and C. Beer<sup>6</sup>

<sup>1</sup>Max Planck Institute for Biogeochemistry, Jena, Germany

<sup>2</sup>Universität Hamburg, Hamburg, Germany

<sup>3</sup>Uni Research Climate, Bjerknes Centre for Climate Research, Bergen, Norway

<sup>4</sup>Max Planck Institute for Meteorology, Hamburg, Germany

<sup>5</sup>Helmholtz Centre Potsdam GFZ German Research Centre for Geosciences, Potsdam, Germany

<sup>6</sup>Stockholm University, Stockholm, Sweden

*Correspondence to:* S. Kaiser (skaiser@bgc-jena.mpg.de)

**Abstract.** A detailed process-based methane module for a global land surface scheme has been developed which is general enough to be applied in permafrost regions as well as wetlands outside permafrost areas. Methane production, oxidation and transport by ebullition, diffusion and plants are represented. In this model, oxygen has been explicitly incorporated in diffusion, transport by plants  
5 and two oxidation processes, of which one uses soil oxygen, while the other uses oxygen that is available via roots. Permafrost and wetland soils show special behaviour, such as variable soil pore space due to freezing and thawing or water table depths due to changing soil water content. This has been integrated directly into the methane-related processes. A detailed application at the polygonal tundra site Samoylov, Lena delta, Russia, is used for evaluation purposes. The application at Samoylov also  
10 shows differences in the importance of the several transport processes and in the methane dynamics under varying soil moisture, ice and temperature conditions during different seasons and on different microsites. These microsites are the elevated moist polygonal rim and the depressed wet polygonal center. The evaluation shows sufficiently good agreement with field observations despite the fact that the module has not been specifically calibrated to these data. This methane module is designed  
15 such that the advanced land surface scheme is able to model recent and future methane fluxes from periglacial landscapes across scales. In addition, the methane contribution to carbon cycle – climate feedback mechanisms can be quantified when running coupled to an atmospheric model.

## 1 Introduction

Knowledge on atmospheric methane concentrations is a key factor in several global scale environmental research fields. Besides acting as a highly potent greenhouse gas and thus influencing global  
20 climate change, methane also contributes to degrading the ozone layer. Its average atmospheric lifetime is about 12.4 years, and its current atmospheric concentration in the Arctic is about 1850 ppbV

(Ito and Inatomi, 2012). Concentrations have been reported to rise slowly but steadily since the onset of industrialisation, and, after a hiatus at the beginning of the 21st century, have recently be found  
25 to rise again. These recent dynamics in the global atmospheric methane budget are still not fully explained, emphasising the fact that also future trajectories of methane and its role in global climate change are highly uncertain. The global warming potential of methane is 84 to 86 times that of carbon dioxide over an integration period of 20 years and 28 to 34 times over 100 years (Myhre et al., 2013). Accordingly, even though its absolute mixing ratios are quite low compared to carbon  
30 dioxide, it makes up for about 20 % of the radiative forcing from all greenhouse gases. Thus, for the radiation balance and the chemistry of the atmosphere, it is important to understand land–atmosphere exchanges of methane.

Environmental conditions are highly heterogeneous in permafrost regions, where landscapes are  
35 often characterised by small-scale mosaics of wet and dry surfaces. The heterogeneous aerobic and anaerobic conditions in permafrost soils, in concert with elevated soil carbon stocks (Hugelius et al., 2014), set the conditions for large and spatially heterogeneous methane emissions in these areas (Schneider et al., 2009). Such strongly varying environmental and soil conditions as well as processes that influence the methane production and emissions are challenges in a process-oriented  
40 model with a bottom-up approach for methane balance estimation. However, process-based modelling approaches are powerful tools that help to quantify recent and future methane fluxes at large spatial scale and over long time periods in such remote areas. They can give first estimates where field measurements are missing and help to understand the effects of climate change on permafrost methane emissions. In addition, the effect of methane emissions on climate, hence feedback mech-  
45 anisms, can be analysed using an Earth system model. For such purposes, a methane module for an Earth system model has to be process-based and working under most environmental conditions, including permafrost.

Currently existing process-based methane models have been usually developed for applications in  
50 temperate or tropical wetlands, without considering permafrost-specific biogeophysical processes, such as e.g. freezing and thawing soil processes, (e.g. Zhu et al., 2014; Schuldt et al., 2013). In other cases, they are embedded within a vegetation model, which cannot easily be coupled to an atmospheric model, (e.g. Schaefer et al., 2011; Wania et al., 2010; Zhuang et al., 2004). Some models have been developed only for small-scale applications (e.g. Xu et al., 2015; Mi et al., 2014;  
55 Khvorostyanov et al., 2008; Walter and Heimann, 2000) or use an empirical approach (e.g. Riley et al., 2011). Highly simplified models might be less reliable for global applications (e.g. Jansson and Karlberg, 2011; Christensen et al., 1996) because of oversimplification in simulating the complexity of the methane processes.

60 The aim of this study is to introduce a new methane module that is running as part of a land surface scheme of an Earth system model. Moreover, it shall be general enough for global applications, including terrestrial permafrost ecosystems. The methane module presented in this work represents the gas production, oxidation and relevant transport processes in a process-based fashion. Among other processes, this new methane module takes into account the size variation of the pore spaces  
65 in the soil column in relation to the freezing and thawing cycles, influencing directly the methane concentration in the soil. Furthermore, in this model the oxygen content is explicitly taken into account, enabling two process-based oxidation processes: bulk soil methane oxidation and rhizospheric methane oxidation.

70 The platform chosen to develop the methane module is the land surface scheme JSBACH (Jena Scheme for Biosphere Atmosphere Coupling in Hamburg) of the MPI-ESM (Max Planck Institute Earth System Model). The starting point was a model version that has a carbon balance (Reick et al., 2013), a five layer hydrology (Hagemann and Stacke, 2015) and includes permafrost as described in Ekici et al. (2014). A parallel development by Schuldt et al. (2013) incorporated wetland carbon  
75 cycle dynamics and was also integrated in the model version presented in this work. The basis for the methane-related processes were the works by Walter and Heimann (2000) and Wania et al. (2010). Special focus was also put on the connections with permafrost and wetland as well as the explicit consideration of oxygen. This paper describes the newly developed methane module, and for the purpose of model evaluation it presents an application at a typical polygonal tundra site in northeast  
80 Siberia.

## 2 Methods

### 2.1 Site description

For the purpose of evaluation, this model has been applied at the site Samoylov Island, located 120 km south of the Arctic Ocean in the Lena River Delta in Yakutia with an elevation of 10 to 16 m  
85 above sea level. The mesorelief of Samoylov Island is flat, while as microrelief, there are low-center polygons with the soil surface about 0.5 m higher at the rim than at the center. This results in different hydrological conditions, also influencing heat conduction. The average maximum active layer depth at the dryer but still moist polygonal rims and the wet polygonal centers is at about 0.5 m (Boike et al., 2013). While the water table at the polygonal rims is generally well below the soil  
90 surface, the polygonal centers are often water saturated with water tables at or above the soil surface (Sachs et al., 2008).

The vegetation on Samoylov Island can be classified as wet polygonal tundra that is composed of mosses, lichens and vascular plants. According to Kutzbach et al. (2004), mosses and lichens grow

95 about 5 cm high and cover about 95 %, while vascular plants grow about 20 to 30 cm high and cover  
about 30 % of the area. The most dominant vascular plant, both at the rim and at the center, is *Carex*  
*aquatilis* but with dominance of only 8 % at the rim compared to 25 % at the center. However, most  
of the species present at the rim are different from those present at the center. According to Sachs  
et al. (2010), the proportions of moist and wet microsites are approximately 65 % moist and 35 %  
100 wet. The reader is referred to Sachs et al. (2010) for more details on the study site. Below, moist  
microsites will be referred to as rim and wet microsites as center.

## 2.2 Methane module description

### 2.2.1 Layer structure

For a numerically stable representation of gas transport processes in soils, a much finer vertical soil  
105 structure is required than what is normally used for thermal and hydrological processes in JSBACH.  
Therefore, a new soil layering scheme has been implemented for the methane module. This scheme  
is variable and allows fine layers (in the order of a few cm) but still inherits the hydrological and  
thermal information contained in the coarse scheme. Number and height of layers can be chosen  
arbitrarily, allowing also non-equidistant solutions.

110

Internally, the module uses midpoints and lower boundaries of the layers as well as distances be-  
tween the midpoints. At the bottom, the layering scheme is truncated at depth to bedrock. The layers,  
where the

- plant roots end, i.e., rooting depth lies,
- 115 – water table lies and
- minimum daily water table over the previous year lies (permanent saturated depth),

have also been determined. These layers have a specific function for methane production and various  
transport processes. Details will be given below in the respective sections (see also App. A1).

120 For model evaluation, fine layers with a height of 10 cm have been used. For all the layers of the new  
soil layering scheme, the soil temperature is interpolated linearly from the coarse JSBACH layering  
scheme. From these values, also the previous day's mean soil temperature is calculated. In addition  
to geometry and soil temperature, each layer has its own hydrological parameters, as described in  
the next section, and various state variables describing the different gases' concentrations.

### 125 2.2.2 Hydrology

For the fine layers, several hydrological values have to be determined using the relative soil moisture  
and ice content from the coarse JSBACH layering scheme. Fine scale layer values are derived such

that known values at common layers are kept and only those layers that span more than one input layer get values of the weighted mean of the involved coarse layer values. The relative soil water content is then defined by the sum of the relative soil moisture and ice content.

Subtracting the relative ice content from the volumetric soil porosity leads to the ice-corrected volumetric soil porosity. With this, the relative moisture content of the ice-free pores can be defined, which is calculated by division of the relative soil moisture content by the ice-corrected volumetric soil porosity. Finally, the relative air content of the ice-free pores is defined as one minus the relative moisture content of the ice-free pores.

The water table is calculated following Stieglitz et al. (1997). From the uppermost soil layer, the water table is located in the immediate layer above the first one with a relative soil water content of at least 90 % of field capacity. This definition was used because the current hydrology scheme in JSBACH does not allow to consider water content of soils higher than field capacity, or standing water (Hagemann and Stacke, 2015). Instead, water content exceeding field capacity is removed by runoff and drainage. In this context, the current model implementation considers only mineral soil (field capacity: 0.435; porosity: 0.448), i.e. no peat layers exist in this version. The dimensionless but ice-uncorrected field capacity is used because the relative soil water content already includes ice. The water table depth is then defined as

$$w = \begin{cases} b, & \text{if } r_w \leq 0.7 \cdot fc \\ b - \frac{r_w - 0.7 \cdot fc}{fc - 0.7 \cdot fc} \cdot h, & \text{if } r_w > 0.7 \cdot fc \end{cases} \quad (1)$$

Here,  $b$  is the lower boundary of the soil layer of interest with height  $h$  and relative soil water content  $r_w$ .  $fc$  is the field capacity. If even the uppermost layer has a relative soil water content of at least 90 % field capacity, the water table is located at the surface. The mean water table of the previous day is used where appropriate to keep consistency with the daily time step of the carbon decomposition routine. The minimum of this daily mean water table over the previous 365 days is used as the permanently saturated depth.

At a given time step, the soil column, that contains the water table depth and the permanently saturated depth, is divided into three strata that are from the top:

- the unsaturated zone above the water table,
- the saturated zone below the water table (located above the annual minimum water table depth) and
- the permanently saturated zone (located below the annual minimum water table depth).

Evidently, this stratification is hydrological, while the layering scheme is purely numerical. Thus, each stratum may contain several soil layers. For carbon decomposition, the mean temperatures of

the previous day at the midpoints of these three strata are needed. These values are derived analogously to the temperatures in the fine layers by interpolating the mean temperatures of the previous day linearly.

With these three strata, carbon that may experience unsaturated conditions is split into an unsaturated and a saturated pool by the water table. In addition, a permanently saturated carbon pool is defined by the permanently saturated depth. This scheme is similar to what Schuldt et al. (2013) proposed. Further details about the calculation of the carbon decomposition are given in App. A2.

### 2.2.3 Production

Initial values of methane and oxygen concentrations have been derived using reported gas concentrations in free air for oxygen and methane. For oxygen, the global mean value for 2012 is used ( $8.56 \text{ mol m}^{-3}$ , <http://cdiac.ornl.gov/tracegases.html>). The value for methane is defined as the March 2012 value ( $77.06 \text{ } \mu\text{mol m}^{-3}$ , <http://agage.eas.gatech.edu/data.htm>).

The initial gas concentrations in the soil profile are determined assuming equilibrium condition between free ambient air as well as the air and moisture in the soil pore space. Thus, Henry's law with the dimensionless Henry constant is applied. The dimensionless Henry constant is defined as the ratio of the concentration of gas in moisture to its concentration in air (Sander, 1999). The chosen temperature dependence values, which are  $d(\ln k_{H\text{CH}_4}) (d(T^{-1}))^{-1} = 1900 \text{ K}$  and  $d(\ln k_{H\text{O}_2}) (d(T^{-1}))^{-1} = 1700 \text{ K}$ , as well as the Henry constants at standard temperature, which are  $k_{H\text{CH}_4}^{25} = 0.0013 \text{ mol dm}^{-3} \text{ atm}^{-1}$  and  $k_{H\text{O}_2}^{25} = 0.0013 \text{ mol dm}^{-3} \text{ atm}^{-1}$ , are all from Dean (1992).

The calculated initial values for methane and oxygen concentrations in the soil profile can be transformed into gas amounts and vice versa. During methane transport process calculation, concentration values are widely used. In between time steps, however, the volume of ice is recalculated and therefore the relative ice-free pore volume changes. Thus, concentration values also change, but only the gas amounts stay constant. Therefore, at the beginning of each methane module execution, the total gas amounts that have been saved at the end of the previous time step are divided by the current relative ice free pore volume to recalculate the current concentration values.

The final products of the decomposition of soil carbon are carbon dioxide and methane. Depending on the soil hydrological conditions, carbon dioxide or methane are produced from the decomposing carbon pools that belong to the three strata described above. These decomposition results are distributed over fine-scale layers of the whole soil column. Because no direct vertical information about the amount of decomposing carbon is available, equal decomposition velocity in all layers of

one stratum is assumed. Thus, once the decomposed amount of carbon per stratum is known, the  
 200 decomposed amount of carbon per layer per stratum depends on the amount of available carbon in  
 that layer only. And the carbon content in the soil layers for Samoylov has been prescribed from  
 measurements by Zubrzycki et al. (2013), Harden et al. (2012) and Schirrmeister et al. (2011), tak-  
 ing local horizontal variations of polygonal ground (Sachs et al., 2010) into account (see App. A3).

205 The initial amount of carbon in the pools is obtained from the sum of carbon in each layer of the  
 strata. In this case, the first and second stratum share one carbon pool which is split after calculation  
 of the mean water table over the previous day. The amount of carbon per layer is divided by the  
 amount of carbon per stratum. These weights are used for distributing the amounts of decomposed  
 210 carbon from strata to layers. In addition, the share of initially produced carbon dioxide and methane  
 is set assuming all decomposed carbon above the water table and half of it below the water table gets  
 carbon dioxide,

$$c_{prod}^{CH_4} = 0.5 \cdot \frac{f_C}{\sum_{sl} f_C} \cdot \frac{C_s}{h \cdot v_p} \quad (2)$$

Here,  $sl$  means all layers in the stratum, and  $C_s$  is the decomposed carbon in the stratum.  $f_C$  is the  
 soil carbon content of the layer with height  $h$ , and  $v_p$  is the ice-corrected volumetric soil porosity.  
 215 Mass conservation is done if the stratum is too small to get a layer assigned, so that the associated  
 carbon is not neglected. The gas fluxes for methane and carbon dioxide are calculated via the sums  
 of the respective amounts, and the produced gases are added to their respective pools in the layers.

#### 2.2.4 Bulk soil methane oxidation

Only part of the oxygen in the soil is assumed to be available for methane oxidation. In layers above  
 220 the mean water table over the previous day, available oxygen is reduced by the amount that corre-  
 sponds to the amount of carbon dioxide which is produced by heterotrophic respiration but not more  
 than 40 % of the total oxygen content. Additional 10 % of oxygen is assumed to be unavailable  
 and also reduced. In layers below the water table, the amount of oxygen is reduced by 50 %. This  
 approach is similar to Wania et al. (2010).

225

For methane oxidation itself, a Michaelis–Menten kinetics model is applied. The  $Q_{10}$  temperature  
 coefficient is similar to the one used by Walter and Heimann (2000) but with a reference temper-  
 ature of 10 °C rather than the annual mean soil temperature. Reaction velocities of both, methane  
 and oxygen, are taken into account by using an additional equivalent term with the concentration of  
 230 oxygen and  $K_m^{O_2} = 2 \text{ mol m}^{-3}$ , which is chosen to be the average concentration of oxygen at the  
 water table. Furthermore, methane and oxygen follow a prescribed stoichiometry,

$$c_{oxid}^{CH_4} = \min \left( V_{max} \cdot \frac{c^{CH_4}}{K_m^{CH_4} + c^{CH_4}} \cdot \frac{c^{O_2}}{K_m^{O_2} + c^{O_2}} \cdot Q_{10}^{\frac{T-10}{10}} \cdot dt, 2 \cdot c^{O_2}, c^{CH_4} \right) \quad (3)$$

$c$  denotes the concentration of oxygen or methane in the layer.  $T$  is the soil temperature in the layer, and  $dt$  is the time step. The total gas fluxes for methane, oxygen and carbon dioxide are again  
235 calculated as the sums of the respective amounts.

### 2.2.5 Ebullition

The implementation of the ebullition of methane follows largely the scheme from Wania (2007). Ebullition is the transport of gas via bubbles that form in liquid water within the soil and transport methane rapidly from their place of origin to the water table. The amount of methane to be released  
240 through ebullition is determined by that amount of the present methane that can be solute in the present liquid water. This amount depends on the overall amount of methane present in the layer but also on the storage capacity of the present liquid water.

In a first step, the concentration of methane in soil air is assumed to be in equilibrium with the  
245 concentration in soil water. Thus, by application of Henry's law, the present methane can be partitioned into the potentially ebullited methane concentration in soil air and the potentially solute methane concentration in soil water. The dimensionless Henry solubilities at current soil temperature conditions are used for this. As initial approximation, all methane is assumed to be in soil air and potentially ebullited. Thus, first, the potentially solute methane in soil water can be determined,  
250 but it will also be overestimated because of this approximation. Therefore, second, an updated potentially ebullited concentration of methane in soil air is determined by subtracting the potentially solute methane from the total methane. Unlike proposed in Wania (2007), these two steps are iterated until stable state conditions are reached.

255 In a second step, to calculate the maximal amount of methane that can be soluble in the present soil water, the Bunsen solubility coefficient from Yamamoto et al. (1976) is applied. By considering the available pore volume, this gives the volume of methane that can maximally be dissolved. The ideal gas law results in the maximally soluble amount of methane. For that, the soil water pressure in layers below the water table needs to be derived. This is determined from soil air pressure and  
260 the pressure of the water column, using the basic equation of hydrostatics. For this, the specific gas constant of moist air and the soil air pressure in layers above the water table are required. For the air pressure calculation, the barometric formula is used. Hereby, the first layer uses the air pressure at the soil surface and deeper layers use the above layer's soil air pressure. The specific gas constant of moist air finally needs the saturation vapour pressure and relative soil air moisture, both in layers  
265 above the water table. The former is calculated after Sonntag and Heinze (1982), and the latter is set to 1 if the relative water content is at least at the wilting point and to 0.9 elsewhere.

Now, the maximally soluble concentration of methane is derived by dividing the maximally soluble

amount of methane by the available pore volume. Thus, the concentration of methane that is solute  
 270 and in equilibrium with methane in the air is the lesser of the following two concentrations: the po-  
 tentially solute methane, that was calculated in the first step, and the maximally soluble methane, that  
 was calculated in the second step. Finally, the actually ebullited methane is the difference between  
 all methane and solute methane,

$$c_{ebul}^{CH_4} = c^{CH_4} - \min \left( k_{H\ CH_4} \cdot c_{gas}^{CH_4}, \frac{\beta \cdot p_w}{R \cdot T} \right), \quad (4)$$

275 with  $k_{H\ CH_4}$  being the Henry solubility,  $c_{gas}^{CH_4}$  the methane concentration that can potentially be ebul-  
 lited,  $\beta$  the Bunsen solubility coefficient,  $p_w$  the soil water pressure and  $T$  the soil temperature, all  
 of the layer, and  $R$  is the gas constant.

The ebullited methane is removed from the layers and, if the water table is below the surface, added  
 280 to the first layer above the water table. In this case, the ebullition flux to atmosphere is zero, and the  
 methane is still subject to other transport or oxidation processes in the soil. Otherwise, if the water  
 table is at the surface and if snow is not hindering, it is added to the flux to atmosphere. Snow is  
 assumed not to hinder if snow depth is less than 5 cm. If, finally, the water table is at the surface but  
 285 snow is hindering, ebullited methane is put into the first layer and the ebullition flux to atmosphere  
 is zero like in the first case.

### 2.2.6 Diffusion

For the diffusion of methane and oxygen, Fick's second law with variable diffusion coefficients  
 is applied. The possibility of a non-equidistant layering scheme is specifically taken into account.  
 Diffusion is a molecular motion due to a concentration gradient, with a net flux from high to low  
 290 concentrations. For soil as a porous medium, moreover with changing pore volumes because of dif-  
 ferent contents of ice, the ice-corrected soil porosity of the layers also has to be accounted for in  
 the equation system directly as a factor (Schikora, 2012). The discretisation of the computational  
 system is done with the Crank–Nicholson scheme with weighted harmonic means for the diffusion  
 coefficients. While ice is treated as non-permeable for gases, the diffusion is allowed to continue if  
 295 the soil is frozen but not at field capacity, i.e., there is no simple cut at 0 °C. During every model  
 time step of 1 hour, two half-hourly diffusion steps are calculated to prevent instabilities like os-  
 cillations or unrealistic behaviour like negative concentrations. The diffusion specific time step can  
 be decreased further if necessary and if an adjustment of the layering scheme is not desired. The  
 possibility of these effects results from the tight connection between layering scheme, time step and  
 300 diffusion coefficients.

As initial condition, free ambient air, soil air and moisture phase are assumed to be in equilibrium.  
 The boundary condition at the bottom of the soil column is always of Neumann type, i.e., no flux is

assumed. At the top of the soil column, boundary conditions are assumed to depend on snow depth.

305 If there are at least 5 cm of snow, no flux is assumed, and therefore Neumann type is applied also at the top. However, if there are less than 5 cm of snow, ambient air conditions are assumed to hold at the boundary, and therefore Dirichlet type with gas concentration in free air is applied,

$$v_p \cdot \frac{\partial c}{\partial t} = \frac{\partial}{\partial x} \left( D \cdot \frac{\partial c}{\partial x} \right) ; \quad c = c_{air} , \quad x \in \Gamma_D ; \quad \frac{\partial c}{\partial x} = 0 , \quad x \in \Gamma_N . \quad (5)$$

Here,  $v_p$  is the volumetric soil porosity,  $c$  denotes the gas concentration,  $t$  is the time,  $x$  is the depth, 310  $D$  denotes the diffusion coefficient,  $\Gamma_D$  is the boundary with Dirichlet type boundary conditions, and  $\Gamma_N$  is the boundary with Neumann type boundary conditions. For details on how the diffusion coefficients are determined, see App. A4. The solution of the diffusion equation system is obtained by the `tridag_ser` and `tridag_par` routines from Press et al. (1996) in Numerical Recipes.

315 By subtracting the gas concentrations after diffusion from those before for methane and vice versa for oxygen, concentration changes are derived with positive values for lost methane and gained oxygen. Multiplying the concentration changes with their respective pore volumes as usual and summing the resulting amounts over the layers gives the total fluxes of methane and oxygen.

### 2.2.7 Plant transport

320 Gas transport via plants is first calculated for oxygen entering the soil. Then, another oxidation mechanism with this newly gained oxygen takes place (see Sect. 2.2.8). After that, the transport of methane via plants is modelled. The transport via plants happens through the plant tissue that contains big air filled channels, the aerenchyma, to foster aeration of the plant's roots. However, because plants need the oxygen that reaches their roots for themselves, their root exodermis acts as efficient 325 barrier against gas exchange.

In this model configuration, gas transported by plants is assumed to happen only via the phenology type grass with C3 photosynthetic pathway. The contribution to methane emissions due to the degradation of labile root exudates is not taken into account here. The potential role of this process 330 is reviewed in the discussion section. Furthermore, the gas transport via plants will occur only if snow is not hindering, i.e., if there are less than 5 cm of snow. This is justified by the consideration of snow crinkling the culms such that transport is not possible anymore. A diffusion process from aerenchyma through the root tissue to soil is assumed as key process, and it is described by Fick's first law. Gas transport is fast inside the air-filled aerenchyma, hence, atmospheric air conditions can 335 be assumed there.

The diffusion flux via the plants is determined from the oxygen concentration gradient between ambient air and the root zone soil layers. The diffusion coefficients of methane and oxygen in the

exodermis are unknown but can be assumed to be slightly lower than in water (e.g. Kutzbach et al., 2004; Končalová, 1990). Therefore, their values are set to be 80 % of their respective values in soil water at the given soil temperatures and pressures,  $D_r = 0.8 \cdot D_w$ .

The oxygen flux entering the soil is furthermore constrained by the surface area of root tissue,  $A_r^{ges} = A_r \cdot q_p$ , which is determined from the surface area of a single plant's roots,  $A_r = l_r \cdot d_r \cdot \pi$ , multiplied by plant density,  $q_p = \frac{t_{ph}}{t_p}$ . Here,  $l_r$  is the root length,  $d_r$  the root diameter, both in metres,  $t_{ph}$  the number of tillers per square metre depending on phenology, and  $t_p$  the number of tillers per plant. Finally, the number of tillers per square metre is influenced by plant phenology, which is determined from the  $LAI$ , using  $t_{ph} = \max(t_m) \cdot \frac{LAI}{\max(LAI)}$ , with  $t_m$  being the number of tillers per square metre. Please see also App. A5.

350

The root tissue is assumed to be distributed equally between all root-containing layers, thus  $A_r^{rl} = A_r^{ges} \cdot \frac{h}{\sum_{r,l} h}$ , with  $h$  denoting the layer height and  $rl$  all layers with roots. The travel distance,  $dx$ , is set to the thickness of the exodermis in metres because this is the limiting factor. The plant transport per layer is thus modelled as

$$355 \quad n_{plant}^{O_2} = D_r^{O_2} \cdot (c_{air}^{O_2} - c^{O_2}) \cdot \frac{1}{dx} \cdot dt \cdot A_r^{rl} . \quad (6)$$

Here,  $c_{air}^{O_2}$  is the concentration of oxygen in free air and  $dt$  the time step length. For every soil layer, the resulting amount of oxygen is converted into concentration and added to the oxygen pool. As usual, the flux of oxygen into the soil is calculated by the total soil column balance.

360 After plant transport of oxygen, additional methane can be oxidised by the amount of oxygen that leaves the roots (Sect. 2.2.8). The remaining methane is then available for plant transport, which is modelled exactly as for oxygen, with one exception: It is necessary to account for the fraction of roots able to transport gases,  $f_r = \frac{dom_{Carex\ A.}}{dom_{vascular\ P.}}$ . This can be thought of as a measure of distance between the methane and the transporting roots. With increasing amounts of roots being able to

365 transport gases, the distance for methane to travel to them is getting smaller and transport is generally enhanced. To account for that,  $f_r$  is set for rim and center, respectively, as the fraction of the dominance measure for *Carex aquatilis* divided by the dominance of vascular plants (Kutzbach et al., 2004). The plant transport of methane is thus modelled as

$$n_{plant}^{CH_4} = D_r^{CH_4} \cdot (c^{CH_4} - c_{air}^{CH_4}) \cdot \frac{1}{dx} \cdot dt \cdot A_r^{rl} \cdot f_r . \quad (7)$$

370 The variables definitions are the same as for oxygen and  $c_{air}^{CH_4}$  is the concentration of methane in free air. A similar effect will be taken into account for oxygen when it is allowed to oxidise only methane near the transporting roots. To determine the flux out of the soil, the differences of methane concentrations in the soil subtracted by the concentration in ambient air are used. For every layer,

the amount of methane is converted into concentration and removed from the methane pool. Again,  
 375 the total methane flux out of the soil is calculated by summing up individual layer balances.

### 2.2.8 Rhizospheric methane oxidation

The oxygen gained by the transport via plants is assumed to foster methane oxidation next to their  
 roots. Thus, if oxygen is leaving these roots, the same oxidation routine as described above in Sect.  
 2.2.4 is applied to calculate how much additional methane is oxidised by this oxygen. Obviously,  
 380 only gas concentrations in layers with roots will be influenced. Because the amount of vegetation  
 with roots that are able to supply oxygen varies between rim and center, the dominance measure ( $f_r$   
 from Sect. 2.2.7) is applied again as a factor to account for the distance to these roots,

$$c_{plox}^{CH_4} = \min \left( V_{max} \cdot \frac{f_r \cdot c^{CH_4}}{K_m^{CH_4} + f_r \cdot c^{CH_4}} \cdot \frac{c_{plant}^{O_2}}{K_m^{O_2} + c_{plant}^{O_2}} \cdot Q_{10}^{\frac{T-10}{10}} \cdot dt, 2 \cdot c_{plant}^{O_2} \cdot f_r \cdot c^{CH_4} \right). \quad (8)$$

The variables' definitions are the same as for the bulk soil methane oxidation,  $f_r$  is the fraction of  
 385 roots in the layer that are able to transport gases, and  $c_{plant}^{O_2}$  is the concentration of oxygen trans-  
 ported by plants. Carbon and oxygen pools are adjusted accordingly. The total exchange with the  
 atmosphere is determined by summing the total amount of gas that is calculated by multiplying the  
 concentrations by their pore space.

## 2.3 Simulation setup

390 As a global land surface scheme, the JSBACH model is set up for spatially explicit model runs at  
 larger scales. Accordingly, many assumptions behind the model structures are only valid at large  
 spatial scales. One prominent example here is the hydrology scheme, which works exclusively ver-  
 tically, therefore cannot represent lateral water flow from rim to center, which is a process of major  
 importance in polygonal tundra sites. Other examples include assumptions regarding e.g. the mod-  
 395 ules for radiation scheme and energy balance (no south- versus north-facing slopes etc.). Since our  
 ultimate target is to provide a new methane module that can be integrated into global scale JSBACH  
 simulations, accordingly the structure of our methane module also needs to target spatially explicit  
 experiments. Thus, the site level runs presented here are landscape-scale spatial runs with a grid cell  
 size of  $0.5^\circ$  using input data representing a very small domain.

400

To still facilitate site-level simulations that capture the general hydrologic characteristics of a polyg-  
 onal tundra site, we split the model experiments into two separate runs, one for rim and one for  
 center. A redistribution of excess water from the rim area into polygon centers was added in order to  
 mimic lateral flow. In more detail, the performed experiment consisted of two simulation runs with  
 405 different settings for rim and center. The polygon rim is assumed to be a normal upland soil, and a  
 standard JSBACH simulation run was performed. For the polygon center, runoff and drainage of the  
 rim have been collected and added to center precipitation. Additionally, for the center run, runoff

and drainage have been switched off until the soil water content reached field capacity.

410 The sequence of methane processes executed in the module is identical to the above described order  
within Sect. 2.2.1 to 2.2.8, and has been sorted according to the velocity of the specific processes,  
from fast to slow. The impact of changing this sequence on total and component methane flux rates  
was tested in a separate sensitivity study (not shown). These tests indicated only a minor influence  
of the sequence to the partitioning of the fluxes between the transport processes compared to the  
415 influence of hydrology or the definition of the processes themselves. Still, it cannot be ruled out that  
modelled methane processes may be modified through the chosen order under certain conditions.

The carbon pools for rim and center were initialised using data from Zubrzycki et al. (2013) and  
information from Harden et al. (2012), Schirrmeister et al. (2011) and Sachs et al. (2010). The used  
420 values for rim and center for Samoylov are  $627.61 \text{ mol m}^{-2}$  and  $731.94 \text{ mol m}^{-2}$  for the upper  
carbon pool (i.e. the two zones making up the unsaturated and temporarily saturated soil layers)  
and  $16355 \text{ mol m}^{-2}$  and  $25424 \text{ mol m}^{-2}$  for the lower carbon pool (i.e. the permanently saturated  
zone). Because of the lack of information on how the modelled soil carbon from these two pools is  
distributed vertically, a depth distribution is applied to the decomposed carbon instead. For all layers  
425 within one stratum, equal decomposition velocity is assumed. The relative amounts of measured car-  
bon are applied as distribution aid for the decomposed carbon. The layers used were 10 cm in height.  
The only further settings varying between rim and center are two vegetation parameters required for  
the process of plant transport, i.e. the number of tillers per square metre, and the dominance of *Carex*  
*aquatilis*. Beyond the definitions cited above, the model has not been calibrated to site specific pro-  
430 cesses or properties.

To initialise hydrological conditions, a spin-up of 100 years was done using one single year of  
climate data with average conditions from the period of observations. Starting in year 41 of this  
spin-up, the methane processes were activated. This setup was chosen to stabilize the hydrological  
435 conditions before the methane processes were included. After finalising the spin-up, the time period  
of interest has been calculated with actual climate data.

## 2.4 Sensitivity experiments

We reviewed the list of parameters that are required to run the new methane module of JSBACH  
and categorised them by relevance and available information to support the chosen settings. Based  
440 on this survey, we identified a shortlist of 10 parameters, which are listed in Table 2. To allow for  
a uniform processing of all parameters on this list, we assumed an uncertainty range of +/- 10 %  
for each of these settings. Changing each parameter by these percentages and performing for each  
of those an individual model run yielded a range of resulting methane emissions according to the

influence of each parameter. Model sensitivity towards the setting of the chosen parameters was  
445 evaluated through changes in the cumulative methane emissions over the modelled time period that  
followed the variation of the parameter.

## 2.5 Forcing and evaluation data

The climate forcing data used in the simulations is the same as in Ekici et al. (2014), spanning from  
450 14 July 2003 to 11 October 2005. The climate input consists of air temperature, precipitation, at-  
mospheric relative humidity, short and long wave downward radiation and wind speed, all at hourly  
resolution.

For model evaluation, data from chamber measurements has been used. This data was collected  
455 over 39 days from July to September 2006 by Sachs et al. (2010), resulting in 55 single measure-  
ments for the rim and 48 for the center. In addition, eddy covariance based fluxes from Wille et al.  
(2008) have been used, integrating rim and center. From this, 3340 data points were available for the  
simulation time period.

## 3 Results

### 460 3.1 Modelled water table and permanent saturated depth

The modelled depth of permanent saturation for both, rim and center, is always at the same level of  
31.9 cm. In contrast, the modelled water table changes during the seasons for rim and center dif-  
ferently (Fig. 1). In general, it is higher at the center than at the rim, though there are few cases in  
early spring when the rim has a higher water table than the center. This results from the different soil  
465 water contents at the rim and at the center which were forced by adding runoff and drainage from  
the rim to the center as precipitation and prohibiting runoff and drainage at the center until the soil  
water content reached field capacity. Still, in the early part of the thawing season, the water tables at  
the rim and at the center are similar. While in general, at the rim, the water table is highest during the  
early thawing season, at the center, there is a tendency to high values towards the end of the thawing  
470 season. But if the rim shows a high water table, there will generally also be a high water table at the  
center. Overall, the water table in the model is changing relatively quickly, due to the quick changes  
in modelled soil water conditions.

However, JSBACH does not allow to model soil water content higher than field capacity, or standing  
475 water at the surface. Thus, the maximal soil water content in the model is field capacity. It is obvious,  
that there is a mismatch with the real situation in the field, where the center is often water saturated  
with water tables at or above the soil surface. While measurements of the water table at the rim give

values between 35 and 39 cm (Kutzbach et al., 2004), the mean summer value in the model is 30.88 cm. For the center, measurements give values between -12 and 17 cm (Sachs et al., 2010), while the  
480 mean summer value in the model is 24.52 cm. Hence, the model tends to have a slightly higher water table at the rim, but the calculated water table is too low at the center. Still, this water table has been calculated using the unsaturated soil water content. For the interpretation of the methane module results, it therefore has to be taken into consideration that JSBACH is currently not capable to fill the entire pore space up to saturation with water, i.e. a realistic representation of saturated water content  
485 in the field is not possible.

For additional results concerning modelled physical conditions, such as soil moisture and ice content as well as soil temperatures, the reader is referred to App. B1 to B3.

### 3.2 Modelled methane flux in summer and winter

490 The modelled methane fluxes at rim and center are different for the different seasons (Fig. 2). While most of the modelled flux is positive (i.e. emission to the atmosphere), there are also uptake events. The spread of the flux is greater for the center than for the rim in both summer and winter. While the majority of flux values in summer is positive at the center, it is more balanced at the rim. In winter, the methane flux is almost always zero, following the assumption that snow may hinder the exchange.  
495 However, at the center, there are some rare events when uptake takes place. In the mixed approach, which means 65 % rim and 35 % center, the overall mean emission is about  $0.0813 \text{ mgC m}^{-2} \text{ h}^{-1}$  for the summer period. The overall higher emissions at the center are due to higher moisture and thus more favourable conditions for methane production in concert with lower methane oxidation rates.

### 3.3 Role of different transport processes

500 During most part of the year, the diffusive methane flux is rather small at the rim (Fig. 3A) and sometimes slightly negative at the center (Fig. 3B). The largest methane emissions, both at the rim and at the center, occur during spring. In this season, the methane that is produced in the top soil from late autumn on and accumulated during winter is released in the form of so-called spring bursts upon snow thaw.

505

Plant mediated methane transport is smaller than diffusion but more pronounced at the center than at the rim (Fig. 3A and 3B) because plant transport was defined to be slower than diffusion in water and it should thus lead to lower emissions under less wet conditions. Despite the exodermis is a very thin layer, it is an efficient barrier against gas exchange, maintaining gases such as oxygen that are  
510 necessary for metabolic processes inside the roots. Thus, the diffusion rate through roots is slower than through water, and in turn, diffusion in water is much slower than diffusion in air. Moreover, the soils in the center were not water saturated in the model, promoting diffusive methane released

though coarse pores. Under wet soil conditions, plant transport is dominant relative to diffusion, because diffusion in water is a slower process. At the center, ebullition is the most important process (Fig. 3B) while diffusion at the rim (Fig. 3A). This is due to the drier conditions at the rim that allow a fast diffusion through air, while ebullition is only possible under conditions of high water content. Because in the model, higher soil moisture is calculated from the middle to the end of the thawing season, most of the emissions by ebullition and plant transport occur at the center (Fig. 3B).

In the mixed approach, only the diffusion of the rim alters substantially the pattern of the emissions (Fig. 3C). In total, the polygon center accounts for a 6.8 times as large fraction of emissions as the rim due to the higher methane production under wetter conditions (Fig. 3D). This means, a total share of 78.6 % of the methane emissions in the mixed approach is coming from the center. Emissions at the rim are highest during spring, while they are highest at the center during the mid and late season (Fig. 3D).

When comparing the total fluxes of the center to the ones of the rim, diffusion is almost doubled, plant transport is 19 times as high, and ebullition is 18 times as high (Table 1). This results in almost seven times higher total methane emissions at the center than at the rim. At the rim diffusion is more than 13 times as high as plant transport, while at the center it is just slightly higher than plant transport. Ebullition is about 4.5 times as high as plant transport both at the rim and at the center. These differences are again due to the differences in soil moisture content, which allow more production under higher soil moisture and leads to more methane emissions. Thus, under drier conditions, diffusion in air will transport the main portion of gas, and under wetter conditions plant transport may increase relative to diffusion. With reduced soil air, the remaining velocity of the diffusion is almost the same order of magnitude than the overall velocity of plant transport, in contrast to the velocity of diffusion mainly through air.

Not only splitting the total methane flux into several transport processes allows evaluating the relative contribution of each process linked to rim or center characteristics, but also it is possible to analyse differences in temporal patterns (Fig. 4A). As noted above, at the rim the fluxes are much lower than at the center (Fig. 4B) because less methane is produced under drier conditions, or methane becomes oxidised in the soil column. Ebullition makes up a large portion of the total budget at both microsites at isolated time steps, reflecting the nature of this process, while its total amount for rim is rather small over longer timeframes. At the rim, diffusion represents both the second largest methane release and substantial uptake during the season (Fig. 4A). The smallest flux portion at the rim is due to plant transport, which also shows some uptake. In contrast, at the center plant transport plays a much more pronounced role, and diffusion fluxes are more negative. All these effects occur in the different hydrological regimes at the rim and at the center.

550

Furthermore, ebullition can only take place in soils with high soil moisture content, and this is more common at the center than at the rim. Consequently, substantially more ebullition is found at the center than at the rim. In the mixed approach, diffusion accounts for about 2.5 times of the emissions of plant transport, while ebullition accounts for 4.5 times of it. Overall, 0.588 g of carbon are emitted by each square metre during the modelled time period from 14 July 2003 to 11 October 2005.

### 3.4 Parameter sensitivity tests

Results of the sensitivity tests are summarised in Table 2 and indicate that just one of the chosen parameters,  $\text{fracCH4Anox}$ , has a major influence on the cumulative methane emissions when varied within a 10 % range.  $\text{fracCH4Anox}$  represents the fraction of methane produced under anaerobic conditions compared to the total decomposition flux. For two more parameters,  $\text{fracO2forOx} + \text{fracO2forPh}$  and  $\text{KmO2}$ , the net effect was still larger than 1 percent.  $\text{fracO2forOx} + \text{fracO2forPh}$  influences the available amount of oxygen for the methane oxidation, whereas  $\text{KmO2}$  influences the oxidation as Michaelis–Menten constant for oxygen. For all remaining parameters, only negligible effects on the cumulative methane emissions were found.

### 3.5 Production versus oxidation

Methane oxidation follows the pattern of methane production as long as enough oxygen is available (Fig. 5A). Production, and hence also oxidation, is higher during times of more moist conditions for both, the rim and the center, and also higher for the center than for the rim (Fig. 5B). At the center, a substantial amount of methane is oxidised in the rhizosphere with oxygen that enters the soil via plant transport. This happens when a high amount of methane is produced, which is rather rare at the rim due to lower soil moisture (Fig. 5A). During spring, bursts of oxidation occur both at the rim and at the center because methane produced during the winter and stored below the snow gets in contact with oxygen. The different moisture and temperature regimes at the rim and the center and their dynamics determine these results.

### 3.6 Comparison to chamber measurements

Although the number of available field data is small and from a different year than the meteorological forcing data, the field measurements and model results are of the same order of magnitude (Fig. 6). Observations and model results show higher center values compared to the rim, but the model seems to underestimate occasional uptake events. For the rim, the model gives methane fluxes to the atmosphere between  $-0.0237$  and  $39.3 \text{ mgC m}^{-2} \text{ h}^{-1}$  with mean  $0.0267 \text{ mgC m}^{-2} \text{ h}^{-1}$ , while the available field measurement values range from  $-0.111$  to  $0.881 \text{ mgC m}^{-2} \text{ h}^{-1}$  with mean  $0.154 \text{ mgC m}^{-2} \text{ h}^{-1}$ . For the center, the model gives values between  $-0.0189$  and  $86.8 \text{ mgC m}^{-2} \text{ h}^{-1}$  with

mean  $0.231 \text{ mgC m}^{-2} \text{ h}^{-1}$ , while the available field measurement values range from  $-0.0584$  to  $1.22$   
585  $\text{mgC m}^{-2} \text{ h}^{-1}$  with mean  $0.327 \text{ mgC m}^{-2} \text{ h}^{-1}$ . Besides higher mean values, the extremes are thus  
lower for the field measurements. This is due to the observation period excluding spring time when  
the model calculates the highest emissions in the form of spring bursts.

One should also take into account that JSBACH is a global model, therefore it requires input param-  
590 eters from global fields. Furthermore, other modules of JSBACH, like the hydrology or the carbon  
decomposition, are adjusted for global applications. Therefore, JSBACH integrates processes over  
much larger grid cell areas than what chamber measurements may represent. Hydrological condi-  
tions and other processes are highly variable in polygonal tundra environments and are of crucial  
importance for methane processes. Still, they may not be represented with the required detail by  
595 the model so that the modelled conditions are the same as those at the measurement site. Thus, it  
is obvious, that with coarser and different hydrological conditions, the modelled methane fluxes per  
square metre for a  $0.5^\circ$  grid cell cannot be identical to the point measurements of chambers. Partic-  
ularly, the low soil moisture in the hydrological conditions of the model may explain the lower mean  
modelled methane fluxes compared to what is reported by chamber data.

### 600 3.7 Comparison to eddy measurements

Eddy covariance data had the best available data coverage of field measurements (light grey areas  
in Fig. 7). Overall model results are of the same order of magnitude as observations, but there are  
also seasonal shifts between model results and measurements. This is due to a mismatch between  
the real soil conditions at the measurement site and the modelled soil climate and hydrology that  
605 cannot be expected to be the same as those in the field. The range of available measurements in  
the modelled period is  $0.0233$  to  $4.59 \text{ mgC m}^{-2} \text{ h}^{-1}$  with mean  $0.609 \text{ mgC m}^{-2} \text{ h}^{-1}$ . The range of  
modelled summer methane emissions in this time frame is  $-0.023$  to  $30.4 \text{ mgC m}^{-2} \text{ h}^{-1}$  with mean  
 $0.0813 \text{ mgC m}^{-2} \text{ h}^{-1}$ . If less than  $5 \text{ cm}$  of snow are on the ground, this is defined as summer time.  
Besides lower mean values, the model shows higher extremes.

610

For this comparison, the same constraints hold like for the comparison to chamber data. The mod-  
elled fluxes differ from field measurements because of differences in thermal or hydrological condi-  
tions. Critical are periods where observations show substantial methane emissions while at the same  
time model results only show minor emissions, e.g. in autumn 2003 or spring 2004. During these  
615 periods, modelled soil temperature values below zero and snow cover result in modelled methane  
fluxes of virtually zero, while in reality soils might be warmer and gas diffusion through snow might  
be possible (see discussion section).

Still, Fig. 7 also shows some patterns that are present in both model results and observations, e.g.

620 periods with increasing fluxes that are followed by a sudden decline in the fluxes in a cyclic manner during a single season. These patterns are linked to the changing soil moisture content. Unfortunately only the first season is covered well by field measurements, while the second misses the later part, and the third covers just a part within. The model shows the largest methane emissions during spring upon snow thaw for both rim and center in the form of burst. There is still little evidence  
625 in field measurements of the occurrence and magnitude of spring bursts, and to our knowledge no published data on this effect exists for Samoylov Island. In the discussion section, we briefly review the evidence of spring bursts in other northern wetland areas to evaluate the representativeness of these events in the model results.

630 For additional results concerning modelled oxygen uptake, such as mixed daily sum, seasonally split and cumulative sums as well as transport process split, see App. B4.

#### 4 Discussion

This paper aims to present the structure of a newly developed methane module for the land surface scheme JSBACH and evaluate its general performance against field observations. The new module  
635 itself is completely integrated into the larger framework of the JSBACH model, therefore sensitivity tests can only be conducted using the full model and a clean separation between existing structure and new components is not always possible. The interpretation and discussion of all findings should therefore consider that the functioning of the new methane module is to a large part dependent on, and in many aspects limited by, the performance of the JSBACH model as a whole.

640 The presented methane module determines production, oxidation and transport of methane to the atmosphere. All of these key processes are heavily dependent on soil water status as well as the quality and quantity of carbon in different soil pools. Both of these aspects, i.e. soil hydrology and carbon decomposition, are handled by existing JSBACH modules which were not modified in the  
645 context of the presented study. With an exclusive focus on simulating processes at site-level scale, it may even be possible to upgrade these modules and add some features that would be relevant for the methane processes; however, since our scope was to provide a methane extension for JSBACH that can be applied globally, certain limitations regarding the representation of site level observations need to be taken into account. This situation is even aggravated due to the use of parameter settings  
650 from global fields, i.e. with a coarse spatial resolution that aggregate conditions over larger areas and thus naturally cannot provide the exact details for the field site where the reference fluxes were measured. Such systematic deviations in modelling framework and parameter configuration will generate systematic differences between model output and site level measurements. Accordingly, modelled hydrological conditions and amounts of decomposed carbon need to be considered when comparing

655 modelled methane fluxes to the site level observations and interpreting the spatiotemporal differences.

As mentioned above, the JSBACH hydrology module has been designed for global applications, and is not capable to capture conditions in complex landscapes such as polygonal tundra. Therefore, 660 for the Samoylov site which we used for this site level analysis, the modelled soil climate and hydrology systematically deviate from those found in the field (Beer, 2016). We still chose to work at this site since a highly valuable interdisciplinary dataset could be provided to evaluate different facets of the model output. To adapt the model to represent the complex hydrology, a mixed approach of combining two different model runs was applied. This approximation implies a very simplified representation of the real hydrological conditions and cannot fully offset all site level differences between 665 model simulations and observational datasets. Accordingly, systematic biases need to be considered when interpreting the findings. However, through this approach we could demonstrate the paramount importance of realistic hydrologic boundary conditions for simulations of the methane balance. In many aspects, details in the behaviour of the methane processes are tightly linked to the spatiotemporal variation of hydrological conditions, therefore biases in hydrology are directly projected on 670 the methane processes.

Still, the authors believe that the comparison of methane simulations against selected site level measurements are an important first step to evaluate the overall performance of the new module. It is 675 obvious that the limitations of the observational database employed herein, i.e. using just one single observation site and focusing on the growing season alone, cannot allow for a comprehensive assessment of the newly implemented algorithms. Accordingly, the limited amount of available field measurements from chamber and eddy covariance based fluxes requires a careful interpretation when compared to model results, particularly regarding the evaluation of JSBACH as a process-oriented 680 global biosphere model. For the Arctic domain, methane emissions during shoulder and winter seasons have been shown to add considerably to the full annual budget, an aspect that we cannot evaluate based on the given database. Moreover, the question of temporal representativeness is complicated by the discontinuous nature of the methane fluxes (e.g. Tokida et al., 2007a; Jackowicz-Korczyński et al., 2010; Tagesson et al., 2012). To overcome these limitations, in follow-up studies the authors 685 plan to conduct model evaluations based on longer-term flux measurements, covering full annual cycles for multiple Arctic sites.

Even though we regard eddy covariance based fluxes as the most reliable reference data source for longer-term site-level model evaluation, the influence of microsite variability in the area surrounding 690 the tower clearly poses a challenge here. Particularly with respect to methane fluxes, pronounced variability in the distribution of soil organic matter and water content may lead to a mosaic of differ-

ent source strengths. For the Samoylov domain, which is characterised by polygonal structures, we mimicked the apparent differences between wet (center) and dry (rim) areas through the execution of two model runs with different settings. Still, the footprint composition of the eddy covariance tower  
695 might not match the mixed approach of 65 % rim and 35 % center used for modelling (Sachs et al., 2010). Even though this mixture generally captures the composition of the larger area surrounding the tower, particularly when footprints are smaller during daytime the reduced field of view of the sensors might focus on areas that are wetter or drier than the average. Our concept of combining two separate model runs has to be regarded as an approximation to cope with the hydrological constraints  
700 of a global model on the one hand, and the complex landscape on the other.

The model application for remote permafrost areas may also be limited by the availability of long-term and complete observations of meteorological data to be used as model forcing. Forcing data and methane fluxes are required for the same time period, which optimally lasts over one or more years.  
705 When going towards regional to global applications, this new model might be additionally compared to regional or global atmospheric inversion results (e.g. Bousquet et al., 2011; Berchet et al., 2015) or data-driven upscaling of eddy covariance or chamber based observations (e.g. Christensen et al., 1995; Marushchak et al., 2015).

710 Within the methane module presented in this work, the discretisation as well as the definition of the pore volume are variable. This requires that the time step of calculation and the diffusion coefficients must fit to the thicknesses of the soil layers. If not set up properly, instabilities like oscillations or unrealistic behaviour like negative concentrations may occur. However, since the new methane module has been designed to be flexible in this respect, adjustments can easily be made in case numerical problems arise.  
715

A parameter sensitivity study (section 3.4) shows that only for one parameter the uncertainty of the resulting methane emissions scales linearly with the uncertainty of the parameter. This parameter represents the amount of *in situ* (potential) methane produced under anaerobic conditions compared  
720 to the total *in situ* decomposition flux into carbon dioxide and methane  $\left(\frac{[CH_4]}{([CO_2]+[CH_4])}\right)$ . Based on the stoichiometry of the methanogenesis chemical reaction equation and based on laboratory and field data (Segers, 1998), this parameter was chosen to be 0.5 in equation 2. In other models, this parameter is used as an effective parameter and has been tuned to match ultimate methane and carbon dioxide emissions from soil to the atmosphere in the absence of an explicit representation of oxygen  
725 and hence methanotrophy (Wania et al., 2010).

Regarding our assumptions concerning fluxes or plant transport during wintertime, according to recent findings (Zona et al., 2016; Marushchak et al., 2015) the settings chosen within the context

of this manuscript might be oversimplifying the actual processes in the field. Our mechanism that  
730 prevents methane release once the snow cover reaches a depth of 5 cm is a very crude approximation  
of the snow cover influence. It resulted from biases in the modelled hydrological conditions in win-  
ter, where freezing of relatively dry soils led to oxic soil conditions that facilitated methane transport  
into the soil. The next iteration of the model development will include a more sophisticated, process-  
based representation of methane diffusion through snow. This upgrade, however, needs to be coupled  
735 to a major restructuring of several model components, and thus cannot be reconciled with the model  
version presented within the context of this manuscript.

The implementation of the plant transport follows a mechanistic approach, but its definition is limited  
by the availability of observational evidence on e.g. diffusion velocities. Therefore, the parameter set-  
740 tings used in this study are subject to high uncertainty. The value for the diffusion coefficient in the  
exodermis was chosen to be 80 % of the diffusion coefficient in water (*pers. comm.* C. Knoblauch).  
The subsequent gas transport within the aerenchyma is assumed to be as quick as diffusion in air.  
With this setup, the effective barrier of the root exodermis will limit the plant transport efficiency,  
and therefore act as a dominant control for this emission pathway. The thickness of this barrier has  
745 a large influence on plant transport as well, i.e. a thinner root exodermis would lead to increased  
plant transport. While this parameter is relatively easy to define, the cumulative surface area of all  
gas transporting roots in the soil column is difficult to constrain. Considering our basic assumption  
that plant transport is slower than diffusion in water, the general patterns of flux processes and soil  
moisture for rim and center conditions appear plausible. Regarding the quantitative flux rates, how-  
750 ever, the fraction of the total flux emitted through plant transport in the model tends to be too low.  
With larger root surface leading to increased plant transport, we therefore could use this setting as  
a tuning parameter to improve this issue. But also the oxygen available to consume methane plays  
another modulating role, particularly for plant transport. Accordingly, new observational evidence  
would certainly improve the associated uncertainties, therefore this issue is subject to ongoing in-  
755 vestigations. With the new methane module, designed to be flexible regarding these kind of settings,  
parameter adjustments with respect to newer findings can be easily implemented.

The contribution of labile root exudates to methane production and emission has been largely ne-  
glected in existing model implementations and is also not considered in this model configuration.  
760 This is also an understudied process in field experiments and can only be estimated indirectly. The  
rate of root exudates is linked to the nutrient availability in soils, with more root exudates present  
in plants located in nutrient poor wetland soils (Koelbener et al., 2010). The wetland soils in Arctic  
tundra are known to be nitrogen limited (Melle et al., 2015; Gurevitch et al., 2006). The plant growth  
in the polygonal lowland tundra of Indigirka, Russia, is co-limited by nitrogen and phosphorus and  
765 only about 5 % of the total nitrogen soil content is active in the biological fraction (Beerman et

al., 2015). The presence of vascular plants in Arctic wetlands support the production of highly labile low molecular weight carbon compounds which can promote methane emissions through their methanogenic decomposition (Ström et al., 2012). An indirect evidence of the role of root exudates to methane production in polygonal ponds and water-saturated soils in Samoylov Island is presented  
770 by Knoblauch et al. (2015). The authors found almost 4 fold higher potential methane production rates in vegetated sites compared to the non-vegetated ones, both with the same C and N soil concentrations. Thus, the contribution to methane emissions from wetland soils in Arctic tundra due to the decomposition of root exudates should be taken into account in models. This will allow the understanding of the role of root exudates under present climate conditions. On the other hand, the  
775 potential nutrient mobilisation in soils due to permafrost degradation under climate change (Kuhry et al., 2010) may reduce the role of root exudates to methane emissions. However, the current JSBACH configuration lacks of a full soil nutrient cycle and the assimilation of nutrients by plant roots, as well as the contribution of root exudates to the total methane emissions cannot be modelled at this point.

780

In Samoylov Island, the minimum of modelled daily sums of methane emissions during summer is smaller and the maximum much higher for rim and center compared to measurements published by Kutzbach et al. (2004). However, these observations do not include spring bursts with very short but also very high emissions or even dry phases with small uptake. On the other hand, the mean of  
785 those measurements is 3 times as high for rim and 3.5 times as high for center compared to the modelled daily sums in summer (Table 3). Such high modelled emissions are rather rare when comparing previously published studies, where the general level of modelled values is lower than in observations (Fig. 7).

790 When comparing our model results at Samoylov Island to published results from other high-latitude regions, reasonable agreement is found. Our modelling results are about 40 to 60 % lower than measurements for BOREAS, Canada, and Abisko, Sweden, (Wania et al., 2010). The Lena River Delta region is much colder and drier compared to these sites, suggesting that lower flux rates are indeed reasonable. Furthermore, the Samoylov site is characterised by mineral soils containing substantially  
795 lower organic carbon as substrate for methane production than the organic soils at the BOREAS site and the mire in Abisko. Compared to measurements done by Desyatkin et al. (2009) on a thermokarst terrain at the Lena river near Yakutsk, our mean results are well within the measurement range if comparing our rim to the drier sites, our center to the wetter sites, and our mixed approach to the entire ecosystem (Table 4). However, climate and environmental conditions in this study were very  
800 different from those in observed in Samoylov, thus this comparison can only be regarded as a rough guideline. Nakano et al. (2000) measured methane fluxes at Tiksi near the mouth of the Lena river. While our mean value at rim is 4.5 times as high as the mean measurements in Tiksi, the mean at

the center is 5.5 times as high as our mean value (Table 3). The modelled minimum is lower for the center but comparable for the rim.

805

The large methane spring burst simulated by the model in both rim and center may represent the release of methane that has been accumulated during winter in the topsoil below the snow layer. To our knowledge, there is no observational reference of spring bursts measured in Samoylov Island. However, evidence of these events have been presented for other wetland areas using chambers and eddy covariance measurements, e.g. in north Sweden, Jammet et al. (2015) and Friborg et al. (1997); in Finland, Hargreaves et al. (2001); in north Japan, Tokida et al. (2007b) and in Northeast China, Song et al. (2012). These studies suggest the presence of spring thaw emissions of methane that occur sporadically over short periods in the form of bursts. The magnitude of the spring bursts can exceed the mean summer fluxes by a factor of 2 to 3. Although spring emissions can account for a large share of the total annual fluxes, their occurrence, duration and magnitude are still uncertain. To adequately characterise the spring bursts in Samoylov Island, it is necessary to perform dedicated field measurements during the spring thaw period. These results will then help to evaluate the representativeness of the modelled spring bursts. In future model iterations, the spring bursts will also be evaluated for larger spatial scales.

820

In Zona et al. (2009), several measurements of methane emissions in the Arctic tundra are presented. Despite our mean values are located towards the lower end, our minimum, mean and maximum values fit well within the given range. Bartlett et al. (1992) measured methane fluxes near Bethel in the Yukon–Kuskokwim delta, Alaska. The provided values for upland tundra compare well to our mean and minimum values. However, the model maximum fluxes are higher than the measurement values for upland tundra but still well in the range of measured values for wet meadow, which has higher moisture contents than upland tundra. In fact, the highest values are calculated if soil moisture is highest, so despite more on the lower end of this water logged landscape type's emissions, they fit well also therein. Summarising, the variability of results of this pan-Arctic survey indicates that methane budgets within all these places are influenced by different conditions in terms of weather, hydrology and carbon pools. Accordingly, the good agreement of our modelled values with these references confirm that our results are within a plausible range at the greater picture, but a detailed evaluation cannot be performed without in-depth analysis of the site-level conditions.

835

Regarding the general structure of the JSBACH model, other parts of the land surface scheme require advancements before applying it with the methane module at global scale and over long time periods can be suggested. For example, soil organic matter should be represented vertically resolved (Braakhekke et al., 2011, 2014; Koven et al., 2015; Beer, 2016), with different soil carbon pools and a moisture dependent decomposition. Furthermore, the site hydrology should include water contents

840 above field capacity, and standing water above the surface (Stacke and Hagemann, 2012). We are also aware, however, that it is not the best approach to calculate an empirical water table depth after Stieglitz et al. (1997) from unsaturated soil water conditions. Together with the water table depth, the soil moisture content itself is of great importance to the presented methane module. Still, with this model version, the importance of different processes, their interplay and the influence of climatic or hydrologic drivers can be studied at site level, which is a major step forward. Furthermore, 845 this process-based implementation can be applied at other sites or with another hydrology, and still, the methane-related processes will only depend on the soil conditions. In order to improve the hydrological scheme of the current model version, it would be desirable to use other approaches like TOPMODEL (e.g. Kleinen et al., 2012) that would allow representing the fraction of the inundated 850 area in a model grid cell based on the topography profile. This would provide a modelled wetland extent and a representation of the water table depth in saturated soils, especially for large-scale applications. This step is being considered and will be included in future model iterations. Despite being a complex process model, the interplay of the processes is consistent. Thus, the influence of climate and hydrology on methane fluxes can be studied in detail. Knowing the dominating processes and 855 environmental conditions provide useful information about the complex behaviour of the methane dynamics in permafrost soils. Summarising, a lot of information can be gained from using this model that all may help understand the complex network of drivers, influencing factors and constraints that govern methane balance in periglacial landscapes.

## 5 Conclusions

860 The aim of this study was to develop a more detailed and consistent process-based methane module for a land surface scheme which is also reliable in permafrost ecosystems. Based on previous work by Wania et al. (2010) and Walter and Heimann (2000), the land surface scheme JSBACH of the global Earth system model MPI-ESM has been enhanced for this purpose. The new methane module of JSABCH-methane represents methane production, oxidation and transport. Methane transport 865 has been represented via ebullition, diffusion and plant transport. Oxygen can be transported via diffusion through soil pores and plant tissue (aerenchyma). Two methane oxidation pathways are explicitly described: one takes the amount of soil oxygen into account and the other uses explicitly oxygen that is available via roots (rhizospheric oxidation). All methane-related processes respond to different environmental conditions in their specific ways. They increase or decrease according to 870 their requirements with changing soil moisture, temperature or ice content. The differences between the processes, seasonal differences as well as differences between the microsites rim and center have been shown.

When combined with a module for water-saturated soil conditions like TOPMODEL (e.g. Kleinen et

875 al., 2012), such methane-advanced land surface scheme can be used to estimate the global methane  
land fluxes, including for periglacial landscapes. These regions are rich in soil carbon (Hugelius et  
al., 2014) and show good conditions for methane production (Schneider et al., 2009). However, they  
are often remote and rather hard to investigate. Thus, process-oriented modelling can contribute to  
understand the role of methane emissions as long as widespread and long-term measurements remain  
880 scarce. In addition, the role of methane for future permafrost carbon feedbacks to climate change can  
be studied. For these reasons, the module in this study is highly integrated also with permafrost and  
wetland processes, e.g., changing pore space in the soil because of freezing and thawing or changing  
water table depths due to changing soil water content. In a first comparison with site level field mea-  
surements, sufficiently good agreements could be shown, despite the module has not been adjusted  
885 to site specific processes or features. Coupling such land surface scheme to atmosphere and ocean  
schemes in an Earth system model will provide the basis for studying methane-related feedback  
mechanisms to climate change.

## **6 Authors' contributions**

S. K. developed the model code and performed the simulations. S. K. also designed the whole study  
890 and prepared the manuscript together with C. B., M. G., K. C.-M. and C. K.. Permafrost module  
code and input data have been provided by A. E., and T. K. provided code for the parallel developed  
wetland representation. S. Z., T. S. and C. W. provided field observations.

## **7 Code availability**

The model code used in this work is available upon request for academic and non-commercial use.

## **895 Appendix A: Additional methods**

### **A1 Layer structure – specific layer determination**

Specific layers are determined by comparing the midpoints of the layers to rooting depth, water  
table or minimum daily water table over the previous year, respectively. If one of these lies between  
two layer midpoints, the layer with the upper midpoint is chosen to be the specific layer for that. If  
900 the depth under consideration and the midpoint of a layer are the same, the corresponding layer is  
chosen.

### **A2 Hydrology – decomposition of carbon**

The decomposition of carbon is determined similar to Schuldt et al. (2013) though appropriate tem-  
peratures are used for each of the three strata. Furthermore, the decomposition times for the three

905 carbon pools have been adjusted to ensure that the two pools under partially oxic conditions are relatively stable, neither accumulating nor decomposing great portions within a few years, and the last pool slowly accumulating. In numbers, the former two pools change only about  $1 \text{ mol m}^{-2}$  each within the calculation period from 14 July 2003 to 11 October 2005. The decomposition time scales used are 80, 400 and 30000 years for the unsaturated, currently saturated and permanently saturated  
910 stratum's carbon pool.

Though the rate of organic matter decomposition at the evaluation site is not known, the present-day amount of carbon in the soil is known (Sect. 2.2.3). Considering short time scales only, the above described approach should give reasonable amounts of decomposed carbon in the three strata.  
915 This way, the input to our methane routine, the amount of decomposed carbon per time step in each stratum, is provided daily.

### **A3 Production – soil carbon per layer**

The amount of soil carbon per layer has been prescribed based on measurements for the first metre of the soil profile by Zubrzycki et al. (2013). The values of the six measurement depths were averaged over the sixteen different center respectively six rim cores. These resulting averages have been  
920 interpolated to 1 cm values for rim and center accordingly. The means of the corresponding 1 cm values are then used for the modelling layers within the first metre of the soil profile.

As Zubrzycki et al. (2013) only give values for the first metre, additional information for the rest  
925 of the soil profile is needed. Schirrmeister et al. (2011) give an estimate for Lena delta soil carbon content of  $553.33 \text{ kg m}^{-2}$  with a soil depth of 18.25 m, which is converted in a volumetric estimate of  $30.32 \text{ kg m}^{-3}$ . Harden et al. (2012) give quantitative information about the depth distribution of soil carbon up to 3 m. Horizontal variations are accounted for by a partitioning in 65 % rim and 35 % center (e.g. Sachs et al., 2010).

930 Using this information, values are assigned to the remaining layers so that the overall mean over all layers, rim and center mixed in the proposed partitioning, gives the volumetric estimate gained from Schirrmeister et al. (2011). Hereby, the information from Harden et al. (2012) about the variability over depth, that is a slight decrease up to 1.7 m and a slight increase thereafter, is taken into  
935 account.

As uppermost values for this, at a depth of 1.05 m, the mean of the deepest measured values are taken as  $21.24 \text{ kg m}^{-3}$  for rim and  $35.00 \text{ kg m}^{-3}$  for center. As values at the turning point, in depths of 1.65 to 1.75 m, the ceiled mean values of the first metre are used, which are  $20 \text{ kg m}^{-3}$  for rim  
940 and  $34 \text{ kg m}^{-3}$  for center. In between, the values are interpolated, towards the depth extrapolated

linearly to meet the criterion of overall fitting to the value of Schirrmeyer et al. (2011) as mentioned above.

#### A4 Diffusion – diffusion coefficients

After Collin and Rasmuson (1988), the diffusion coefficients of methane and oxygen in the soil layers are calculated by adding the diffusion coefficients in soil moisture times the dimensionless Henry solubility to the diffusion coefficients in soil air. Both are weighted by the relative pore moisture respective air content, and the ice-corrected soil porosity of the modelling layers is also considered. The exponents for this are estimated with Newton's method. For fast convergence, an appropriate starting value has been chosen, that was found to be 0.62. The dimensionless Henry solubilities for methane and oxygen at the current soil temperatures are applied, and the diffusion coefficients in soil air and moisture are derived.

The diffusion coefficients in soil air can be seen as such in free air at soil temperature and pressure. They are calculated after Massman (1998) from values at the soil surface with over depth variable soil temperature and pressure. The latter one arises from soil air and water pressure. The values of diffusion coefficients in free air at soil surface are calculated from values at 0 °C and 1 atm (Massman, 1998).

The diffusion coefficients in soil moisture can be seen as such in free water at soil temperature and pressure. They are calculated differently for the two gas species. For methane, Jähne et al. (1987) is used, whereas for oxygen, Boudreau (1996) is used with the calculation of the dynamic viscosity of water after Matthaus as quoted by Kukulka et al. (1987),

$$D = \left(1 - \frac{r_m}{v_p}\right)^2 \cdot (v_p - r_m)^{2 \cdot \epsilon_a} \cdot D_{(0,1)}^a \cdot \left(\frac{T}{T_0}\right)^{1.81} \cdot \frac{p_1}{p_s} + k_H \cdot \left(\frac{r_m}{v_p}\right)^2 \cdot r_m^{2 \cdot \epsilon_w} \cdot D^w . \quad (A1)$$

Here,  $r_m$  is the relative soil moisture content,  $v_p$  the ice-corrected volumetric soil porosity,  $\epsilon_a$  and  $\epsilon_w$  the exponents from Collin and Rasmuson (1988) for air and water,  $T$  the soil temperature,  $p_s$  the soil air respective water pressure in atm and  $k_H$  the Henry constant, all of the layer.  $D_{(0,1)}^a$  is the diffusion coefficient in free air at  $T_0 = 273.15\text{K}$  and standard pressure  $p_1 = 1 \text{ atm}$ , and  $D^w$  is the diffusion coefficient in water under the conditions of the layer. The latter two for methane and oxygen are defined as

$$\begin{aligned} D_{\text{CH}_4(0,1)}^a &= 1.952 \cdot 10^{-5} \text{ m}^2 \text{ s}^{-1} , & D_{\text{CH}_4}^w &= A \cdot \exp\left(-\frac{E_a}{R \cdot T}\right) , \\ D_{\text{O}_2(0,1)}^a &= 1.820 \cdot 10^{-5} \text{ m}^2 \text{ s}^{-1} , & D_{\text{O}_2}^w &= \left(0.2604 + 0.006383 \cdot \frac{T}{\mu}\right) \cdot 10^{-9} \text{ m}^2 \text{ s}^{-1} . \end{aligned} \quad (A2)$$

with  $A$  and  $E_a$  from Jähne et al. (1987), and  $R$  being the gas constant.  $T$  is once more the temperature and  $\mu$  the dynamic viscosity of water, both of the layer.

To establish the boundary conditions for the system properly, for both the upper and lower boundary  
975 of the soil column one additional computational point has to be added to the computational system.  
Also for the boundary conditions, but just for computational reasons, two virtual points in the same  
distance from the upper respective lower boundary as the first respective last inner point are needed.  
These points have as properties their location and diffusion coefficient only, which are the same as  
those of the first respective last layer. The layer heights are used as weights for the weighted har-  
980 monic means of the diffusion coefficients at the borders between the layers. Just if boundary points  
are involved, half of the layer heights are used as weights.

#### **A5 Plant transport – setup details**

The thickness of the exodermis is set to 0.06 mm (Kutzbach et al., 2004). The number of tillers per  
square metre for rim and center are given by Kutzbach et al. (2004). The number of tillers per plant is  
985 set to one. While the mean accumulated root length of one plant is derived from Shaver and Billings  
(1975) to be 0.739 m, the root diameter is derived from Kutzbach et al. (2004) to be 1.9 mm.

### **Appendix B: Additional results**

#### **B1 Modelled relative soil moisture content**

The modelled soil moisture content changes seasonally very much. However, because soil water  
990 content is restricted to field capacity, there is also a limit for soil moisture content at field capacity.  
At the rim (Fig. 8A), soil moisture increases in the upper soil part in spring but decreases with  
ongoing thawing season. In contrast, at the center (Fig. 8B), soil moisture increases only slowly in  
spring, but this increase is ongoing until almost the end of the thawing season. This is due to the  
greater amount of ice in the soil, which thaws slowly. On the other hand, the greater input of water  
995 to the center than to the rim as soon as there is runoff created at the rim is a continuous additional  
supply of soil moisture to the center later in the thawing season. With this, the rim is more moist than  
the center in the beginning of the thawing season but drier in the middle and at the end of it (Fig.  
8C). Just in the deeper layers, rim has a little bit more liquid water during the whole thawing season.  
In winter, however, the amount of liquid water is negligible both at the rim and at the center. Thus,  
1000 differences may only be seen in the timing of changes due to thawing respective freezing, which  
both happen earlier at the rim than at the center. Consequently, they result in earlier wetting of the  
rim's soil during spring as well as earlier drying of it during freezing.

#### **B2 Modelled relative soil ice content**

The modelled soil ice content, in contrast, is almost always higher at the center than at the rim.  
1005 Only during freezing in autumn, there is a short period when there is more ice in the uppermost

soil part at the rim than at the center. During the thawing season there generally is very little ice in the upper part of the rim's soil (Fig. 9A), while at the center, small amounts of ice may also occur in this period (Fig. 9B). Both, rim and center, show substantial amounts of ice below 30 cm even during the summer. Furthermore, during spring, while the uppermost part of the soil at the center is already thawed, an accumulation of new ice takes place right below, which thaws shortly after. In general, the upper soil part gets its ice thawed and frozen more slowly and later at the center than at the rim because there is more ice at the center. Below 30 cm, the difference in ice content between rim and center is increasing in summer (Fig. 9C). However, this levels off during freezing, until it reestablishes in winter at a lower level. In winter, the soil part with the least amount of ice is not on top but between 10 and 30 cm both at rim and center.

### **B3 Modelled soil temperature**

The modelled soil temperatures show deeper thawing and higher temperatures during the thawing season at the rim compared to the center (Fig. 10A). In addition, rim temperatures reach lower values in winter. Moreover, the thawing season starts earlier and ends later for the rim than for the center (Fig. 10B). These effects are due to the generally drier soil at the rim compared to the center. Water dampens the amplitude of the temperature change, and in addition, the phase change takes up energy. While the warming to 0 °C occurs quickly, the phase change takes time and the soil can only warm further after the phase change is completed. During freezing, the reverse occurs. The cooling then is faster and to lower temperatures at the rim compared to the center. In general, deeper layers react more slowly and dampened compared to layers close to the surface. At the rim as well as at the center, there are short periods with temperatures below 0 °C even during summer. The highest temperature differences occur during early spring when there is more ice in the ground at the center than at the rim. Thus, the rim can reach the zero curtain easier (Fig. 10C).

### **B4 Modelled oxygen uptake**

#### **B4.1 Mixed daily sum**

The overall pattern of oxygen uptake shows big portions during the early and late thawing season with a reduced uptake during the mid season (Fig. 11). This is the most moist part of the season, and water effectively reduces oxygen diffusion into the soil. There is also some daily variation in the amount of uptake during the thawing season that is connected to the soil moisture content. The wetter the soil, the less oxygen can enter. Because there is high uptake at the beginning and the end of the thawing season, the overall transport of oxygen is more similar for the rim and the center, in contrast to methane, where the center is dominating. In winter, no uptake takes place because snow hinders the exchange.

## B4.2 Seasonal split

1040 The modelled oxygen uptake at the rim and at the center is different for the different seasons (Fig. 12). In summer, the uptake is purely positive and greater for the rim than for the center. Also, the spread of uptake is greater for the rim than for the center. This is again due to the drier conditions that allow more diffusion through air, which is quicker and can thus lead to higher uptake compared to diffusion in water or via plants under the wetter conditions at the center. In winter, the uptake is  
1045 zero, following the assumption that snow hinders the exchange. In the mixed approach, the overall mean uptake is about  $2.21 \text{ gO}_2 \text{ m}^{-2} \text{ h}^{-1}$ .

## B4.3 Cumulative sums

At the rim, diffusion delivers a much greater portion of oxygen than plant transport (Fig. 13A). At the center, both processes provide almost the same amount of oxygen (Fig. 13B). There are no such  
1050 pronounced bursts during spring as for methane. While plant transport is smaller than diffusion for both, rim and center, the difference is much bigger at the rim. At the center, there is more plant transport but less diffusion than at the rim. Diffusion at the rim and plant transport at the center are increasing towards the end of the thawing season. In contrast, diffusion at the center and plant transport at the rim show decreasing contributions towards the end of the thawing season.

1055 In the mixed approach, rim and center add to a relatively uniform increase of oxygen flux by diffusion over the whole thawing season. For plant transport, the mid season increase is highest, with smaller contributions at the beginning and the end of the thawing season (Fig. 13C). This results from the different timing of high soil moisture content at the rim and at the center that compensate  
1060 each other for diffusion. Furthermore, the wetter the soil, the more plant transport relatively to diffusion should occur, because the more water the more is diffusion slowed down. If, moreover, these conditions occur towards the end of the growing season, which is the case at the center, the effect is bigger than if this happens in spring, which is the case at the rim. Still, diffusion accounts for a larger proportion of uptake than plant transport because plant transport was defined to be slower  
1065 than diffusion in water while diffusion in air is rather quick. It might still be, that the plant transport is too low compared to the total uptake because the root surface might have been chosen too small, like the results for the methane emissions suggest. In total, the rim accounts for more oxygen uptake than the center (Fig. 13D), but the difference is not as high as for the methane emissions. While the late season is slightly more important at the rim, it is the early season for the center.

1070 When comparing rim and center total uptake, diffusion gets reduced to about a third at the center compared to the rim, and plant transport gets almost 4 times as high (Table 5). This results in a reduction to less than two-thirds of the overall uptake at the center compared to the rim. While at

the rim, diffusion is almost 12 times as high as plant transport, they are almost at the same level at  
1075 the center. These differences are again due to the differences in soil moisture content. In the mixed  
approach, diffusion accounts for about 4.5 times of the uptake of plant transport. Overall, 16 kg of  
oxygen are taken up by each square metre in the course of the modelled time period.

#### **B4.4 Transport process split**

Splitting the overall oxygen uptake into the transport processes shows differences in the amount of  
1080 their contribution per process, depending on location, but also differences in the pattern (Fig. 14A).  
The uptake is split into different portions between the processes, that are more equal for the center  
(Fig. 14B) but differ a lot for the rim. There, diffusion is responsible for the majority of the uptake. At  
the center, this is only true in the early season and at the freezing. In the mid season, plant transport  
is much higher than diffusion. While the diffusion part is lower at the center than at the rim, the  
1085 opposite is the case for plant transport. In spring, big amounts of oxygen are taken up both at the  
rim and at the center. In the late season, also some small emissions via diffusion occur at the center.  
In general, uptake through diffusion is greater when soil is drier, which is the case for the rim in the  
late and for the center in the early season. While plant transport is more steady at the rim, there are  
pronounced peaks at the center when the soil is wettest. In spring, when the soil is wettest at the rim,  
1090 plants are not yet that far developed that plant transport could increase to similarly high values as at  
the center during the respective times with high soil moisture content.

*Acknowledgements.* This work has been supported by the PAGE21 project, grant agreement number 282700,  
funded by the EC seventh Framework Programme theme FP7-ENV-2011, and the CARBOPERM project, grant  
agreement number 03G0836B, funded by the BMBF (German Ministry for Science and Education). Addi-  
1095 tional support came from the PerCCOM project, grant agreement number PCIG12-GA-2012-333796, funded  
by the EC seventh Framework Programme theme FP7-PEOPLE-2012-CIG, and the AXA Research Fund,  
PDOC\_2012\_W2 campaign, ARF fellowship M. Göckede.

Special thanks go to Uwe-Jens Görke for his interdisciplinary support and to Guido Krämer for his support  
1100 in graphical issues.

## References

- Bartlett, K. B., Crill, P. M., Sass, R. L., Harriss, R. C., Dise, N. B.: Methane emissions from tundra environments in the Yukon-Kuskokwim delta, Alaska, *J. Geophys. Res.*, 97, D15, 16645–16660, doi:10.1029/91JD00610, 1992.
- 1105 Beer, C.: Permafrost Sub-grid Heterogeneity of Soil Properties Key for 3-D Soil Processes and Future Climate Projections, *Front. Earth Sci.*, 4, 1–81, doi:10.3389/feart.2016.00081, 2016.
- Beerman, F., Telteuskoi, A., Fiencke, C., Pfeiffer, E.-M., Kutzbach, L.: Stoichiometric analysis of nutrient availability (N,P,K) within soils of polygonal tundra, *Biogeosciences*, 122, 2, 211–227, doi:10.1007/s10533-014-0037-4, 2015.
- 1110 Berchet, A., Pison, I., Chevallier, F., Paris, J.-D., Bousquet, P., Bonne, J.-L., Arshinov, M. Y., Belan, B. D., Cressot, C., Davydov, D. K., Dlugokencky, E. J., Fofonov, A. V., Galanin, A., Lavrič, J., Machida, T., Parker, R., Sasakawa, M., Spahni, R., Stocker, B. D., Winderlich, J.: Natural and anthropogenic methane fluxes in Eurasia: a mesoscale quantification by generalized atmospheric inversion, *Biogeosciences*, 12, 18, 5393–5414, doi:10.5194/bg-12-5393-2015, 2015.
- 1115 Boike, J., Kattenstroth, B., Abramova, K., Bornemann, N., Chetverova, A., Fedorova, I., Fröb, K., Grigoriev, M., Grüber, M., Kutzbach, L., Langer, M., Minke, M., Muster, S., Piel, K., Pfeiffer, E.-M., Stoof, G., Westermann, S., Wischnewski, K., Wille, C., Hubberten, H.-W.: Baseline characteristics of climate, permafrost and land cover from a new permafrost observatory in the Lena River Delta, Siberia (1998–2011), *Biogeosciences*, 10, 3, 2105–2128, doi:10.5194/bg-10-2105-2013, 2013.
- 1120 Boudreau, B. P.: *Diagenetic Models and their Implementation. Modelling Transport and Reactions in Aquatic Sediments*, Springer, Berlin, doi:10.1007/978-3-642-60421-8, 1997.
- Bousquet, P., Ringeval, B., Pison, I., Dlugokencky, E. J., Brunke, E.-G., Carouge, C., Chevallier, F., Fortems-Cheiney, A., Frankenberg, C., Hauglustaine, D. A., Krummel, P. B., Langenfelds, R. L., Ramonet, M., Schmidt, M., Steele, L. P., Szopa, S., Yver, C., Viovy, N., Ciais, P.: Source attribution of the changes in atmospheric methane for 2006–2008, *Atmos. Chem. Phys.*, 11, 8, 3689–3700, doi:10.5194/acp-11-3689-2011, 2011.
- 1125 Braakhekke, M. C., Beer, C., Hoosbeek, M. R., Reichstein, M., Kruijt, B., Schrupf, M., Kabat, P.: SOMPROF: A vertically explicit soil organic matter model, *Ecological Modelling*, 222, 10, 1712–1730, doi:10.1016/j.ecolmodel.2011.02.015, 2011.
- 1130 Braakhekke, M. C., Beer, C., Schrupf, M., Ekici, A., Ahrens, B., Hoosbeek, M. R., Kruijt, B., Kabat, P., Reichstein, M.: The use of radiocarbon to constrain current and future soil organic matter turnover and transport in a temperate forest, *J. Geophys. Res. Biogeosci.*, 119, 3, 372–391, doi:10.1002/2013JG002420, 2014.
- Christensen, T. R., Jonasson, S., Callaghan, T. V., Havström, M.: Spatial variation in high-latitude methane flux along a transect across Siberian and European tundra environments, *J. Geophys. Res.: Atmospheres* (1984–2012), 100, D10, 21035–21045, doi:10.1029/95JD02145, 1995.
- 1135 Christensen, T. R., Prentice, I. C., Kaplan, J., Haxeltine, A., Sitch, S.: Methane flux from northern wetlands and tundra. An ecosystem source modelling approach, *Tellus B*, 48, 5, 652–661, doi:10.1034/j.1600-0889.1996.t01-4-00004.x, 1996.

- 1140 Collin, M., Rasmuson, A.: A comparison of gas diffusivity models for unsaturated porous media, *Soil Sci. Soc. Am. J.*, 52, 6, 1559–1565, doi:10.2136/sssaj1988.03615995005200060007x, 1988.
- Dean, J. A.: *Lange's Handbook of Chemistry*, McGraw-Hill, Inc., ISBN 0-07-016384-7, 1992.
- Desyatkin, A. R., Takakai, F., Fedorov, P. P., Nikolaeva, M. C., Desyatkin, R. V., Hatano, R.: CH<sub>4</sub> emission from different stages of thermokarst formation in Central Yakutia, East Siberia, *Soil Science Plant Nutr.*, 55, 4, 558–570, doi:10.1111/j.1747-0765.2009.00389.x, 2009.
- 1145 Ekici, A., Beer, C., Hagemann, S., Boike, J., Langer, M., Hauck, C.: Simulating high-latitude permafrost regions by the JSBACH terrestrial ecosystem model, *Geosci. Model Dev.*, 7, 2, 631–647, doi:10.5194/gmd-7-631-2014, 2014.
- Friborg, T., Christensen, T. R., Sogaard, H.: Rapid response of greenhouse gas emission to early thaw in a subarctic mire as shown by micrometeorological techniques, *Geophys. Res. Lett.*, 24, 23, 3061–3064, doi:10.1029/97GL03024, 1997.
- 1150 Gurevitch, J., Scheiner, S. M., Fox, G. A.: *The Ecology of Plants*, 2nd ed., Sinauer Associates, Inc., Sunderland, ISBN: 0878932941, 2006.
- Hagemann, S., Stacke, T.: Impact of the soil hydrology scheme on simulated soil moisture memory, *Clim. Dyn.*, 44, 7, 1731–1750, doi:10.1007/s00382-014-2221-6, 2014.
- 1155 Harden, J. W., Koven, C. D., Ping, C.-L., Hugelius, G., McGuire, A. D., Camill, P., Jorgenson, T., Kuhry, P., Michaelson, G. J., O'Donnell, J. A., Schuur, E. A. G., Tarnocai, C., Johnson, K., Grosse, G.: Field information links permafrost carbon to physical vulnerabilities of thawing, *Geophys. Res. Lett.*, 39, 15, L15704, 1–6, doi:10.1029/2012GL051958, 2012.
- 1160 Hargreaves, K. J., Fowler, D., Pitcairn, C. E. R., Aurela, M.: Annual methane emission from Finnish mires estimated from eddy covariance campaign measurements, *Theor. Appl. Climatol.*, 70, 1, 203–213, doi:10.1007/s007040170015, 2001.
- Hugelius, G., Strauss, J., Zubrzycki, S., Harden, J. W., Schuur, E. A. G., Ping, C.-L., Schirmer, L., Grosse, G., Michaelson, G. J., Koven, C. D., O'Donnell, J. A., Elberling, B., Mishra, U., Camill, P., Yu, Z., Palmtag, J., Kuhry, P.: Estimated stocks of circumpolar permafrost carbon with quantified uncertainty ranges and identified data gaps, *Biogeosciences*, 11, 23, 6573–6593, doi:10.5194/bg-11-6573-2014, 2014.
- 1165 Ito, A., Inatomi, M.: Use of a process-based model for assessing the methane budgets of global terrestrial ecosystems and evaluation of uncertainty, *Biogeosciences*, 9, 2, 759–773, doi:10.5194/bg-9-759-2012, 2012.
- Jackowicz-Korczyński, M., Christensen, T. R., Bäckstrand, K., Crill, P., Friborg, T., Mastepanov, M., Ström, L.: Annual cycle of methane emission from a subarctic peatland, *J. Geophys. Res.*, 115, G2, G02009, 1–10, doi:10.1029/2008JG000913, 2010.
- 1170 Jähne, B., Heinz, G., Dietrich, W.: Measurement of the diffusion coefficients of sparingly soluble gases in water, *J. Geophys. Res.*, 92, C10, 10767–10776, doi:10.1029/JC092iC10p10767, 1987.
- Jammet, M., Crill, P., Dengel, S., Friborg, T.: Large methane emissions from a subarctic lake during spring thaw: Mechanisms and landscape significance, *J. Geophys. Res. Biogeosci.*, 120, 11, 2289–2305, doi:10.1002/2015JG003137, 2015.
- Jansson, P.-E., Karlberg, L.: *COUP Manual*. Coupled heat and mass transfer model for soil-plant-atmosphere systems, [www.coupmodel.com](http://www.coupmodel.com), 2011.

- Khvorostyanov, D. V., Krinner, G., Ciais, P., Heimann, M., Zimov, S. A.: Vulnerability of permafrost carbon  
1180 to global warming. Part I: model description and role of heat generated by organic matter decomposition,  
Tellus B, 60, 2, 250–264, doi:10.1111/j.1600-0889.2007.00333.x, 2008.
- Kleinen, T., Brovkin, V., Schuldt, R. J.: A dynamic model of wetland extent and peat accumulation: results for  
the Holocene, Biogeosciences, 9, 1, 235–248, doi:10.5194/bg-9-235-2012, 2012.
- Knoblauch, C., Spott, O., Eygrafova, S., Kutzbach, L., Pfeiffer, E.-M.: Regulation of methane production, oxi-  
1185 dation, and emission by vascular plants and bryophytes in ponds of the northeast Siberian polygonal tundra,  
J. Geophys. Res., 120, 12, 2525–2541, doi:10.1002/2015JG003053, 2015.
- Koelbener, A., Ström, L., Edwards, P. J., Venterink, H. O.: Plant species from mesotrophic wetlands cause  
relatively high methane emissions from peat soils, Plant Soil, 326, 1, 147–158, doi:10.1007/s11104-009-  
9989-x, 2010.
- 1190 Končalová, H.: Anatomical adaptations to waterlogging in roots of wetland graminoids: limitations and draw-  
backs, Aquat. Bot., 38, 1, 127–134, doi:10.1016/0304-3770(90)90102-Q, 1990.
- Koven, C. D., Schuur, E. A. G., Schädel, C., Bohn, T. J., Burke, E. J., Chen, G., Chen, X., Ciais, P., Grosse,  
G., Harden, J. W., Hayes, D. J., Hugelius, G., Jafarov, E. E., Krinner, G., Kuhry, P., Lawrence, D. M., Mac-  
Dougall, A. H., Marchenko, S. S., McGuire, A. D., Natali, S. M., Nicolsky, D. J., Olefeldt, D., Peng, S.,  
1195 Romanovsky, V. E., Schaefer, K. M., Strauss, J., Treat, C. C., Turetsky, M.: A simplified, data-constrained  
approach to estimate the permafrost carbon–climate feedback, Phil. Trans. R. Soc. A, 373, 2054, 20140423,  
doi:10.1098/rsta.2014.0423, 2015.
- Kukulka, D. J., Gebhart, B., Mollendorf, J. C.: Thermodynamic and transport properties of pure and saline  
water, Adv. Heat Transfer, 18, 325–363, doi:10.1016/S0065-2717(08)70121-7, 1987.
- 1200 Kuhry, P., Dorrepaal, E., Hugelius, G., Schuur, E. A. G., Tarnocai, C.: Potential remobilization of below-  
ground permafrost carbon under future global warming, Permafrost Periglacial Process., 21, 2, 208–214,  
doi:10.1002/ppp.684, 2010.
- Kutzbach, L., Wagner, D., Pfeiffer, E.-M.: Effect of microrelief and vegetation on methane emis-  
sion from wet polygonal tundra, Lena Delta, Northern Siberia, Biogeochemistry, 69, 3, 341–362,  
1205 doi:10.1023/B:BIOG.0000031053.81520.db, 2004.
- Marushchak, M. E., Friberg, T., Biasi, C., Herbst, M., Johansson, T., Kiepe, I., Liimatainen, M., Lind, S. E.,  
Martikainen, P. J., Virtanen, T., Soegaard, H., Shurpali, N. J.: Methane dynamics in warming tundra of  
Northeast European Russia, Biogeosciences Discussions, 12, 6, 13931–13965, doi:10.5194/bgd-12-13931-  
2015, 2015.
- 1210 Massman, W. J.: A review of the molecular diffusivities of H<sub>2</sub>O, CO<sub>2</sub>, CH<sub>4</sub>, CO, O<sub>3</sub>, SO<sub>2</sub>, NH<sub>3</sub>, N<sub>2</sub>O, NO, and  
NO<sub>2</sub> in air, O<sub>2</sub> and N<sub>2</sub> near STP, Atmos. Environ., 32, 6, 1111–1127, doi:10.1016/S1352-2310(97)00391-9,  
1998.
- Melle, C., Wallenstein, M., Darrouzet-Nardi, A., Weintraub, M. N.: Microbial activity is not always limited by  
nitrogen in Arctic tundra soils, Soil. Biol. Biochem., 90, 1, 52–61, doi:10.1016/j.soilbio.2015.07.023, 2015.
- 1215 Myhre, G., Shindell, D., Bréon, F.-M., Collins, W., Fuglestedt, J., Huang, J., Koch, D., Lamarque, J.-F., Lee,  
D., Mendoza, B., Nakajima, T., Robock, A., Stephens, G., Takemura, T., Zhang, H.: Anthropogenic and  
Natural Radiative Forcing. In: Climate Change 2013: The Physical Science Basis. Contribution of Work-  
ing Group I to the Fifth Assessment Report of the Intergovernmental Panel on Climate Change. Stocker,

- 1220 T.F., Qin, D., Plattner, G.-K., Tignor, M., Allen, S.K., Boschung, J., Nauels, A., Xia, Y., Bex, V., Midgley, P.M. (eds.), Cambridge University Press, Cambridge, United Kingdom and New York, NY, USA, doi:10.1017/CBO9781107415324.018, 2013.
- Mi, Y., van Huissteden, J., Parmentier, F. J. W., Gallagher, A., Budishchev, A., Berridge, C. T., Dolman, A. J.: Improving a plot-scale methane emission model and its performance at a northeastern Siberian tundra site, *Biogeosciences*, 11, 14, 3985–3999, doi:10.5194/bg-11-3985-2014, 2014.
- 1225 Nakano, T., Kuniyoshi, S., Fukuda, M.: Temporal variation in methane emission from tundra wetlands in a permafrost area, northeastern Siberia, *Atm. Env.*, 34, 8, 1205–1213, doi:10.1016/S1352-2310(99)00373-8, 2000.
- Press, W. H., Teukolsky, S. A., Vetterling, W.T., Flannery, B. P.: *Numerical Recipes in Fortran 90. The Art of Parallel Scientific Computing*, 2nd ed., Cambridge University Press, ISBN 0-521-57439-0, 1996.
- 1230 Reick, C. H., Raddatz, T., Brovkin, V., Gayler, V.: Representation of natural and anthropogenic land cover change in MPI-ESM. *J. Adv. Model. Earth Sys.*, 5, 3, 459–482, doi:10.1002/jame.20022, 2013.
- Riley, W. J., Subin, Z. M., Lawrence, D. M., Swenson, S. C., Torn, M. S., Meng, L., Mahowald, N. M., Hess, P.: Barriers to predicting changes in global terrestrial methane fluxes: analyses using CLM4Me, a methane biogeochemistry model integrated in CESM, *Biogeosciences*, 8, 7, 1925–1953, doi:10.5194/bg-8-1925-2011, 1235 2011.
- Sachs, T., Wille, C., Boike, J., Kutzbach, L.: Environmental controls on ecosystem-scale CH<sub>4</sub> emission from polygonal tundra in the Lena River Delta, Siberia, *J. Geophys. Res.*, 113, G3, G00A03, 1–12, doi:10.1029/2007JG000505, 2008.
- Sachs, T., Giebels, M., Boike, J., Kutzbach, L.: Environmental controls on CH<sub>4</sub> emission from polygonal tundra on the microsite scale in the Lena river delta, Siberia, *Global Change Biology*, 16, 11, 3096–3110, 1240 doi:10.1111/j.1365-2486.2010.02232.x, 2010.
- Sander, R.: *Compilation of Henry’s Law Constants for Inorganic and Organic Species of Potential Importance in Environmental Chemistry*, (version 3), <http://www.mpch-mainz.mpg.de/~sander/res/henry.html>, 1999.
- Schaefer, K., Zhang, T., Bruhwiler, L., Barrett, A. P.: Amount and timing of permafrost carbon release in 1245 response to climate warming, *Tellus B*, 63, 2, 165–180, doi:10.1111/j.1600-0889.2011.00527.x, 2011.
- Schikora, J.: *Simulation von Diffusions-Adsorptionsprozessen in natürlichem Gesteinsmaterial mit COMSOL Multiphysics*, (Simulation of diffusion adsorption processes in natural stones material with COMSOL Multiphysics), Diploma thesis, University of Dresden, 2012.
- Schirrmeister, L., Grosse, G., Wetterich, S., Overduin, P. P., Strauss, J., Schuur, E. A. G., Hubberten, H.-W.: 1250 Fossil organic matter characteristics in permafrost deposits of the northeast Siberian Arctic, *J. Geophys. Res.*, 116, G2, G00M02, 1–16, doi:10.1029/2011JG001647, 2011.
- Schneider, J., Grosse, G., Wagner, D.: Land cover classification of tundra environments in the Arctic Lena Delta based on Landsat 7 ETM+ data and its application for upscaling of methane emissions, *Remote Sensing of Environment*, 113, 2, 380–391, doi:10.1016/j.rse.2008.10.013, 2009.
- 1255 Schuldt, R. J., Brovkin, V., Kleinen, T., Winderlich, J.: Modelling Holocene carbon accumulation and methane emissions of boreal wetlands – an Earth system model approach, *Biogeosciences*, 10, 3, 1659–1674, doi:10.5194/bg-10-1659-2013, 2013.

- Shaver, G. R., Billings, W. D.: Root Production and Root Turnover in a Wet Tundra Ecosystem, Barrow, Alaska, *Ecology*, 56, 2, 401–409, doi:10.2307/1934970, 1975.
- 1260 Segers, R.: Methane production and methane consumption: a review of processes underlying wetland methane fluxes, *Biogeochemistry*, 41, 1, 23–51, doi:10.1023/A:1005929032764, 1998.
- Song, C., Xu, X., Sun, X., Tian, H., Sun, L., Miao, Y., Wang, X., Guo, Y.: Large methane emission upon spring thaw from natural wetlands in the northern permafrost region, *Environ. Res. Lett.*, 7, 3, 1–8, doi:10.1088/1748-9326/7/3/034009, 2012.
- 1265 Sonntag, D., Heinze, D.: Sättigungsdampfdruck- und Sättigungsdampfdichtetafeln für Wasser und Eis, (Saturated Vapor Pressure and Saturated Vapor Density Tables for Water and Ice), 1. Aufl., VEB Deutscher Verlag für Grundstoffindustrie, 1982.
- Stacke, T., Hagemann, S.: Development and evaluation of a global dynamical wetlands extent scheme, *Hydrol. Earth Syst. Sci.*, 16, 8, 2915–2933, doi:10.5194/hess-16-2915-2012, 2012.
- 1270 Stieglitz, M., Rind, D., Famiglietti, J., Rosenzweig, C.: An efficient approach to modeling the topographic control of surface hydrology for regional and global climate modeling, *J. Clim.*, 10, 1, 118–137, doi:http://dx.doi.org/10.1175/1520-0442(1997)010<0118:AEATMT>2.0.CO;2, 1997.
- Ström, L., Tagesson, T., Mastepanov, M., Christensen, T. R.: Presence of *Eriophorum schuchzeri* enhances substrate availability and methane emission in an Arctic wetland, *Soil. Biol. Biochem.*, 45, 1, 61–70, doi:10.1016/j.soilbio.2011.09.005, 2012.
- 1275 Tagesson, T., Mölder, M., Mastepanov, M., Sigsgaard, C., Tamstorf, M. P., Lund, M., Falk, J. M., Lindroth, A., Christensen, T. R., Ström, L.: Land-atmosphere exchange of methane from soil thawing to soil freezing in a high-Arctic wet tundra ecosystem, *Global Change Biology*, 18, 6, 1928–1940, doi:10.1111/j.1365-2486.2012.02647.x, 2012.
- 1280 Tokida, T., Miyazaki, T., Mizoguchi, M., Nagata, O., Takakai, F., Kagemoto, A., Hatano, R.: Falling atmospheric pressure as a trigger for methane ebullition from peatland, *Glob. Biogeochem. Cycles*, 21, 2, GB2003, 1–8, doi:10.1029/2006GB002790, 2007.
- Tokida, T., Mizoguchi, M., Miyazaki, T., Kagemoto, A., Nagata, O., Hatano, R.: Episodic release of methane bubbles from peatland during spring thaw, *Chemosphere*, 70, 2, 165–171, doi:10.1016/j.chemosphere.2007.06.042, 2007.
- 1285 Walter, B. P., Heimann M.: A process-based, climate-sensitive model to derive methane emissions from natural wetlands: Application to five wetland sites, sensitivity to model parameters, and climate, *Glob. Biogeochem. Cycles*, 14, 3, 745–765, doi:10.1029/1999GB001204, 2000.
- Wania, R.: Modelling northern peatland land surface processes, vegetation dynamics and methane emissions, PhD thesis, University of Bristol, 2007.
- 1290 Wania, R., Ross, I., Prentice, I. C.: Implementation and evaluation of a new methane model within a dynamic global vegetation model: LPJ-WHyMe v1.3.1., *Geosci. Model Dev.*, 3, 2, 565–584, doi:10.5194/gmd-3-565-2010, 2010.
- Wille, C., Kutzbach, L., Sachs, T., Wagner, D., Pfeiffer, E.-M.: Methane emission from Siberian arctic polygonal tundra: eddy covariance measurements and modeling, *Global Change Biology*, 14, 6, 1395–1408, doi:10.1111/j.1365-2486.2008.01586.x, 2008.

- Xu, X., Elias, D. A., Graham, D. E., Phelps, T. J., Carroll, S. L., Wulfschleger, S. D., Thornton, P. E.: A microbial functional group-based module for simulating methane production and consumption: Application to an incubated permafrost soil, *J. Geophys. Res. Biogeosci.*, 120, 7, 1315–1333, doi:10.1002/2015JG002935, 1300 2015.
- Yamamoto, S., Alcauskas, J. B., Crozier, T. E.: Solubility of methane in distilled water and seawater, *J. Chem. Eng. Data*, 21, 1, 78–80, doi:10.1021/je60068a029, 1976.
- Zubrzycki, S., Kutzbach, L., Grosse, G., Desyatkin, A., Pfeiffer, E.-M.: Organic carbon and total nitrogen stocks in soils of the Lena River Delta, *Biogeosciences* 10, 6, 3507–3524, doi:10.5194/bg-10-3507-2013, 2013.
- 1305 Zhu, Q., Liu, J., Peng, C., Chen, H., Fang, X., Jiang, H., Yang, G., Zhu, D., Wang, W., Zhou, X.: Modelling methane emissions from natural wetlands by development and application of the TRIPLEX-GHG model, *Geosci. Model Dev.*, 7, 3, 981–999, doi:10.5194/gmd-7-981-2014, 2014.
- Zhuang, Q., Melillo, J. M., Kicklighter, D. W., Prinn, R. G., McGuire, A. D., Steudler, P. A., Felzer, B. S., Hu, S.: Methane fluxes between terrestrial ecosystems and the atmosphere at northern high latitudes during 1310 the past century: A retrospective analysis with a process-based biogeochemistry model, *Glob. Biogeochem. Cycles*, 18, 3, GB3010, 1–23, doi:10.1029/2004GB002239, 2004.
- Zona, D., Oechel, W. C., Kochendorfer, J., Paw U, K. T., Salyuk, A. N., Olivas, P. C., Oberbauer, S. F., Lipson, D. A.: Methane fluxes during the initiation of a large-scale water table manipulation experiment in the Alaskan Arctic tundra, *Glob. Biogeochem. Cycles*, 23, 2, GB2013, 1–11, doi:10.1029/2009GB003487, 2009.
- 1315 Zona, D., Gioli, B., Commane, R., Lindaas, J., Wofsy, S. C., Miller, C. E., Dinardo, S. J., Dengel, S., Sweeney, C., Karion, A., Chang, R. Y.-W., Henderson, J. M., Murphy, P. C., Goodrich, J. P., Moreaux, V., Liljedahl, A., Watts, J. D., Kimball, J. S., Lipson, D. A., Oechel, W. C.: Cold season emissions dominate the Arctic tundra methane budget, *PNAS*, 113, 1, 40–45, doi:10.1073/pnas.1516017113, 2016.

**Table 1.** Maximal cumulative methane flux.

|                | Rim    | Center | Mixed  |
|----------------|--------|--------|--------|
| Diffusion      | 0.139  | 0.268  | 0.182  |
| PlantTransport | 0.0103 | 0.196  | 0.0752 |
| Ebullition     | 0.0492 | 0.876  | 0.339  |
| All            | 0.194  | 1.32   | 0.588  |

Maximal values of the cumulative sums of modelled methane flux over the modelled time period for rim, center and a mixed approach of 65 % rim plus 35 % center for the different transport processes and combined in  $\text{gC m}^{-2}$ , rounded to three non-zero digits.

**Table 2.** Methane emission sensitivity towards key parameter settings.

| Parameter                 | lower range | upper range |
|---------------------------|-------------|-------------|
| fracCh4Anox               | -11.966     | 12.035      |
| fracO2forOx+fracO2forPh   | -1.358      | 1.305       |
| KmO2                      | -1.741      | 2.107       |
| snowThresh                | 0.549       | -0.090      |
| resistRoot                | 0.024       | 0.195       |
| thickExoderm              | 0.204       | 0.032       |
| rootLength                | 0.024       | 0.195       |
| rootDiam                  | 0.024       | 0.195       |
| tillerNumberMax           | 0.024       | 0.195       |
| dominanceCarexAquaticilis | -0.151      | 0.344       |

Percentage change of the cumulative methane emissions over the modelled time period, when the parameter was modified by +/-10 %, compared to its default setting.

**Table 3.** Summary of daily methane flux.

|        | Min    | Mean | Max |
|--------|--------|------|-----|
| Rim    | -0.690 | 1.34 | 208 |
| Center | -0.208 | 8.21 | 385 |
| Mixed  | -0.521 | 2.90 | 135 |

Modelled daily methane flux for the summer periods 2003 to 2005 for rim, center and a mixed approach of 65 % rim plus 35 % center in  $\text{mgCH}_4 \text{ m}^{-2} \text{ d}^{-1}$ , rounded to three non-zero digits. Summer means less than 5 cm snow are on the ground. Please note the different unit here.

**Table 4.** Summary of hourly methane flux.

|        | Min     | Mean   | Max  |
|--------|---------|--------|------|
| Rim    | -0.0237 | 0.0267 | 39.3 |
| Center | -0.0189 | 0.231  | 86.8 |
| Mixed  | -0.0235 | 0.0813 | 30.4 |

Modelled hourly methane flux for the summer periods 2003 to 2005 for rim, center and a mixed approach of 65 % rim plus 35 % center in  $\text{mgC m}^{-2} \text{ h}^{-1}$ , rounded to three non-zero digits. Summer means less than 5 cm snow are on the ground.

**Table 5.** Maximal cumulative oxygen uptake.

|                | Rim  | Center | Mixed |
|----------------|------|--------|-------|
| Diffusion      | 17.0 | 5.97   | 13.2  |
| PlantTransport | 1.45 | 5.41   | 2.84  |
| All            | 18.5 | 11.4   | 16.0  |

Maximal values of the cumulative sums of modelled oxygen uptake over the modelled time period for rim, center and a mixed approach of 65 % rim plus 35 % center for the different transport processes and combined in  $\text{kgO}_2 \text{ m}^{-2}$ , rounded to three non-zero digits.

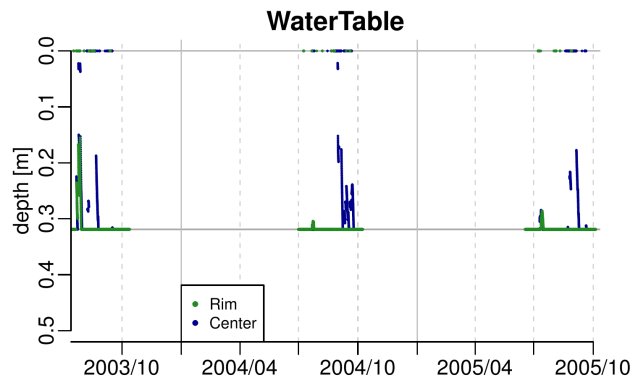


**Figure 1.** Modelled water table at rim and center. Solid lines indicate 1st of January, dashed lines indicate 1st of April, 1st of July and 1st of October of the respective year. Only the summer periods are shown, which means less than 5 cm snow are on the ground.

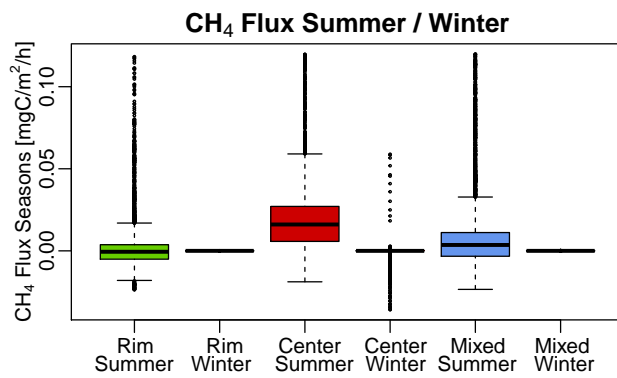


**Figure 2.** Modelled methane flux out of soil at rim, center and a mixed approach of 65 % rim plus 35 % center, split into summer and winter. Summer means less than 5 cm snow are on the ground, winter is the remainder. Because of the widespread of values, from  $-0.0747 \text{ mgC m}^{-2} \text{ h}^{-1}$  to as high as  $86.8 \text{ mgC m}^{-2} \text{ h}^{-1}$ , a portion of 4.66 % values was cut to provide a reasonable picture.

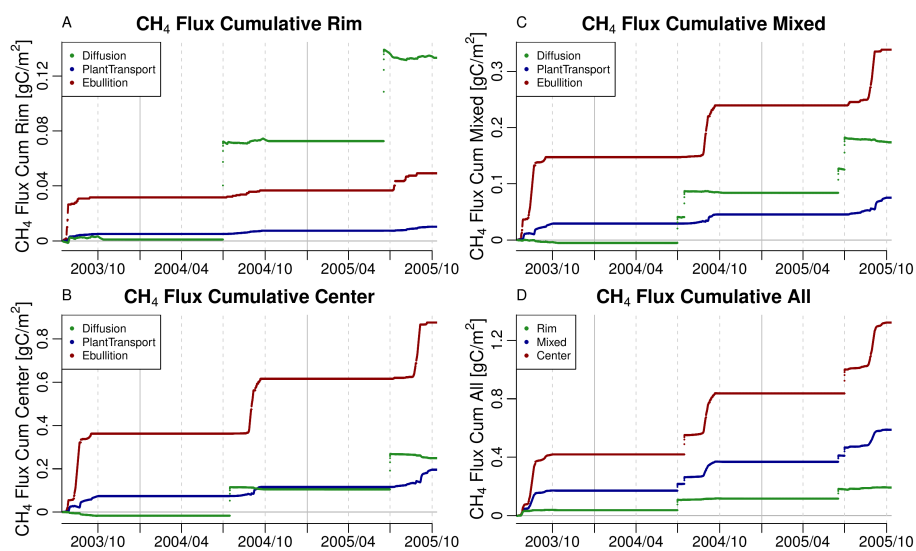


**Figure 3.** Modelled methane flux out of soil at (A) rim, (B) center, (C) a mixed approach of 65 % rim plus 35 % center, split into the different transport processes, and at (D) rim, center and a mixed approach of 65 % rim plus 35 % center, combined, as cumulative sum. Solid lines indicate 1st of January, dashed lines indicate 1st of April, 1st of July and 1st of October of the respective year. Please note the different scales. Table 1 gives the maximal values.

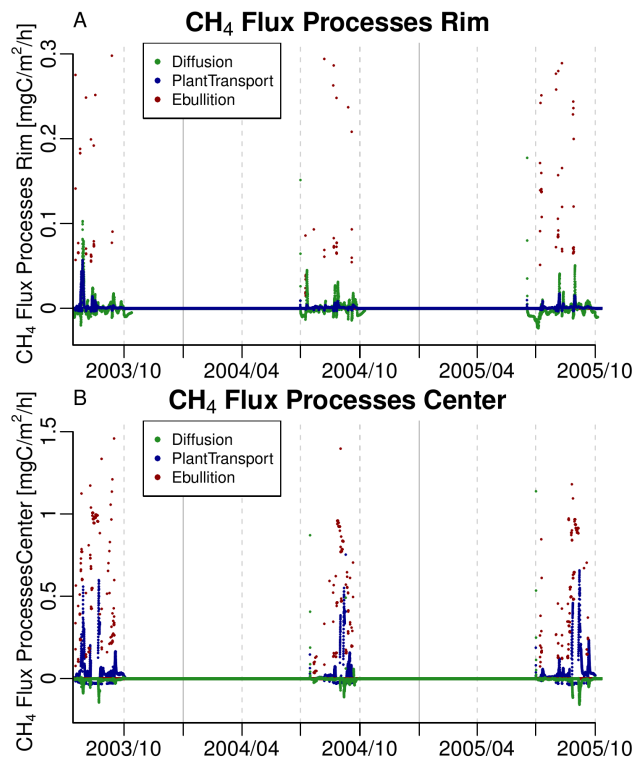


**Figure 4.** Modelled methane flux out of soil at (A) rim and (B) center, split into the different transport processes. Solid lines indicate 1st of January, dashed lines indicate 1st of April, 1st of July and 1st of October of the respective year. Please note the different scales. Because of the widespread of high values, to as high as 39.3 (A) and 86.6 (B)  $\text{mgC m}^{-2} \text{h}^{-1}$ , a portion of 0.108 % (A) and 0.0609 % (B) values was cut to provide reasonable pictures. The minima of the values are -0.0234 (A) and -0.158 (B)  $\text{mgC m}^{-2} \text{h}^{-1}$ .

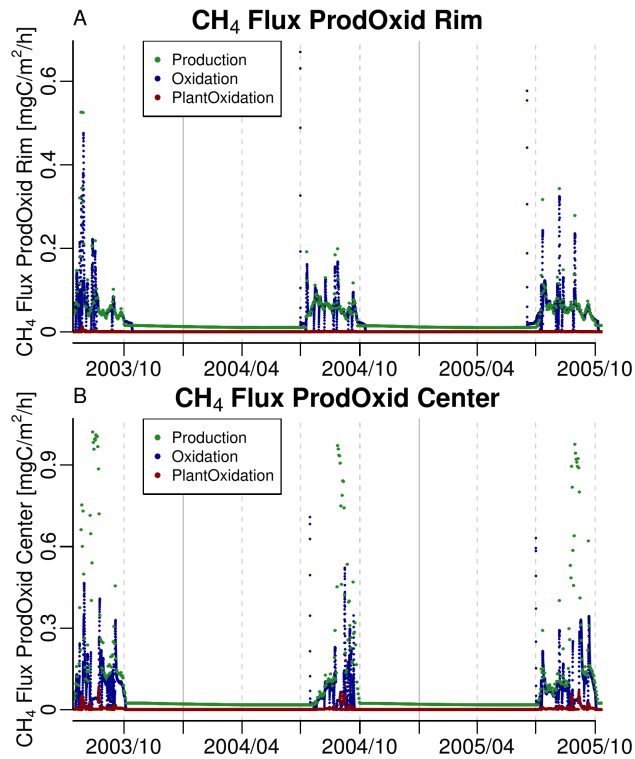


**Figure 5.** Modelled methane amounts that get produced and oxidised at (A) rim and (B) center, split into the different processes. Solid lines indicate 1st of January, dashed lines indicate 1st of April, 1st of July and 1st of October of the respective year. Please note the different scales. The maxima of the values are 0.670 (A) and 1.02 (B)  $\text{mgC m}^{-2} \text{h}^{-1}$ .

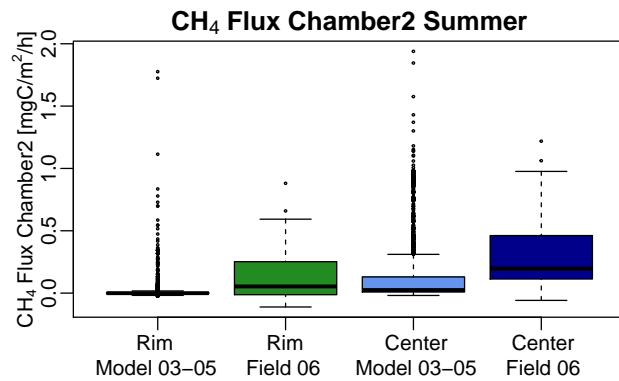


**Figure 6.** Modelled methane flux out of soil at rim and center compared to chamber measurements. Modelled values are only from the summer periods 2003 to 2005, which means less than 5 cm snow are on the ground. Field measurements took place on 39 days from July to September 2006. Because of the widespread of high modelled values, to as high as  $86.8 \text{ mgC m}^{-2} \text{h}^{-1}$ , a portion of 0.347 % modelled values was cut to provide a reasonable picture. The minimum of the modelled values is  $-0.0237 \text{ mgC m}^{-2} \text{h}^{-1}$ .

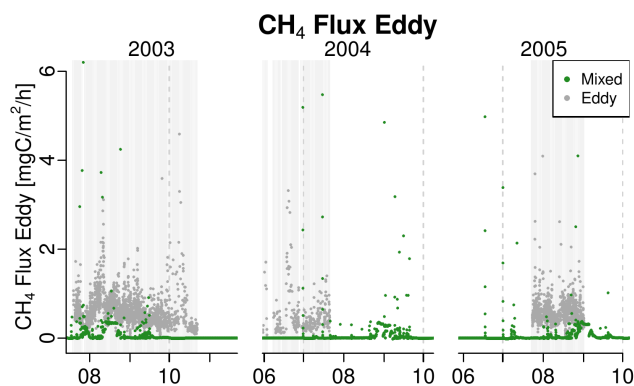


**Figure 7.** Modelled methane flux out of soil in a mixed approach of 65 % rim plus 35 % center compared to eddy covariance measurements. Light grey background indicates measurement data coverage. X-axes indicate 1st day of the respective month of the year. Dashed lines indicate 1st of July and 1st of October of the respective year. Please note the cutouts in-between the different years. Because of the widespread of high modelled values, to as high as  $30.4 \text{ mgC m}^{-2} \text{ h}^{-1}$ , a portion of 0.0507 % modelled values was cut to provide a reasonable picture. The minimum of the modelled values is  $-0.0235 \text{ mgC m}^{-2} \text{ h}^{-1}$ .

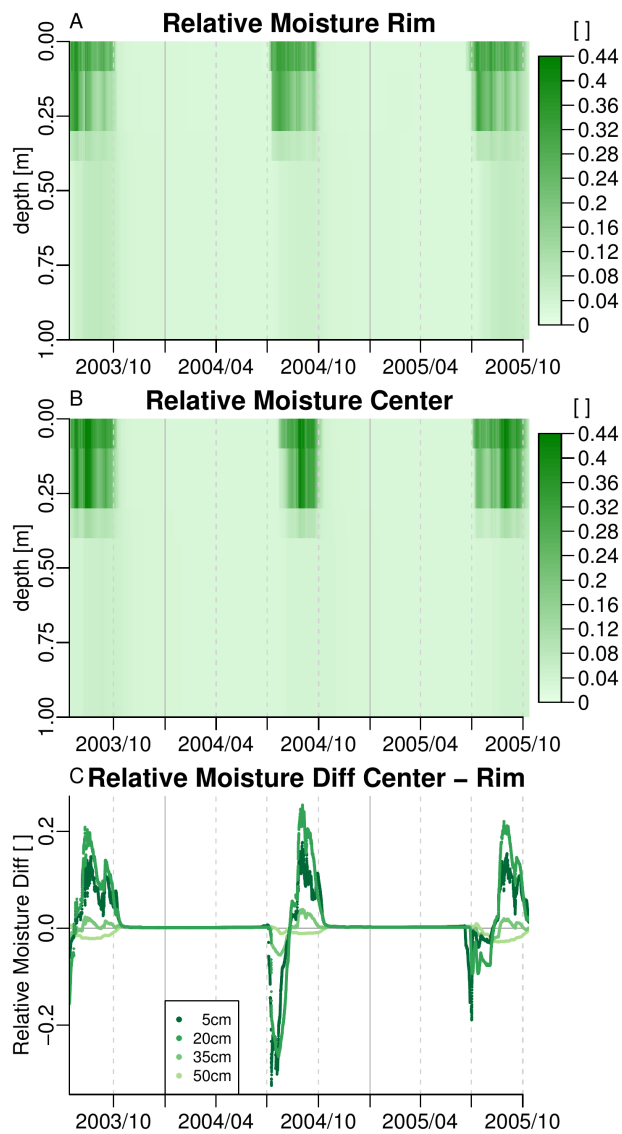


**Figure 8.** Modelled relative soil moisture content of the uppermost metre at (A) rim and (B) center as well as (C) the difference center minus rim in several depths. Solid lines indicate 1st of January, dashed lines indicate 1st of April, 1st of July and 1st of October of the respective year. Scale maximum for (A) and (B) is field capacity, ceiled to two digits.

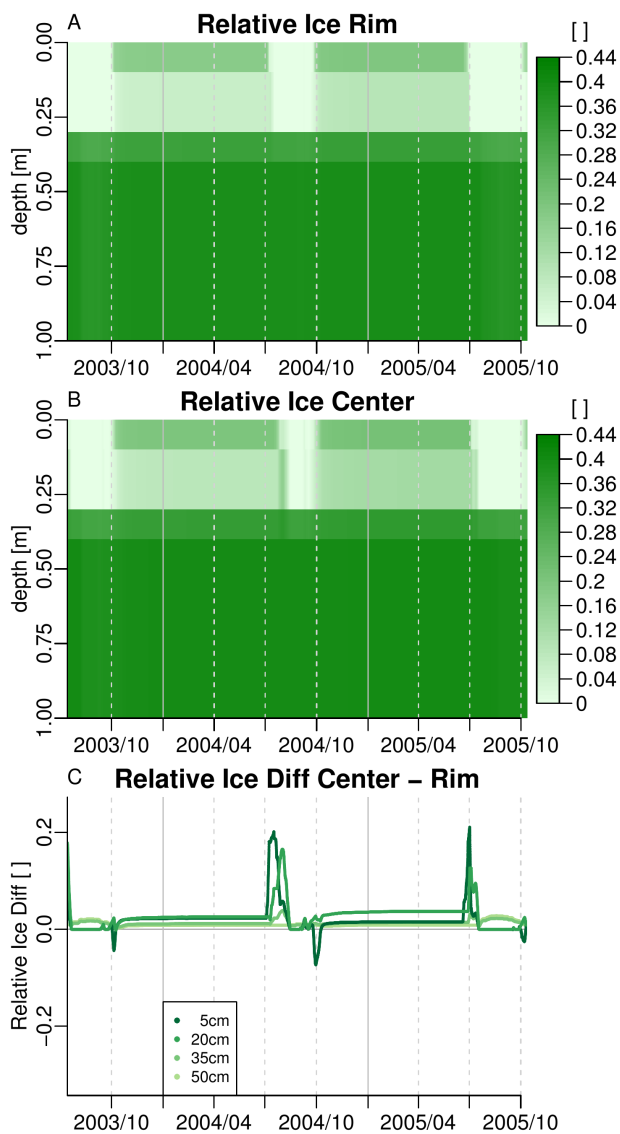


**Figure 9.** Modelled relative soil ice content of the uppermost metre at (A) rim and (B) center as well as (C) the difference center minus rim in several depths. Solid lines indicate 1st of January, dashed lines indicate 1st of April, 1st of July and 1st of October of the respective year. Scale maximum for (A) and (B) is field capacity, ceiled to two digits. The scale for (C) is the same as for the difference of the modelled relative soil moisture content.

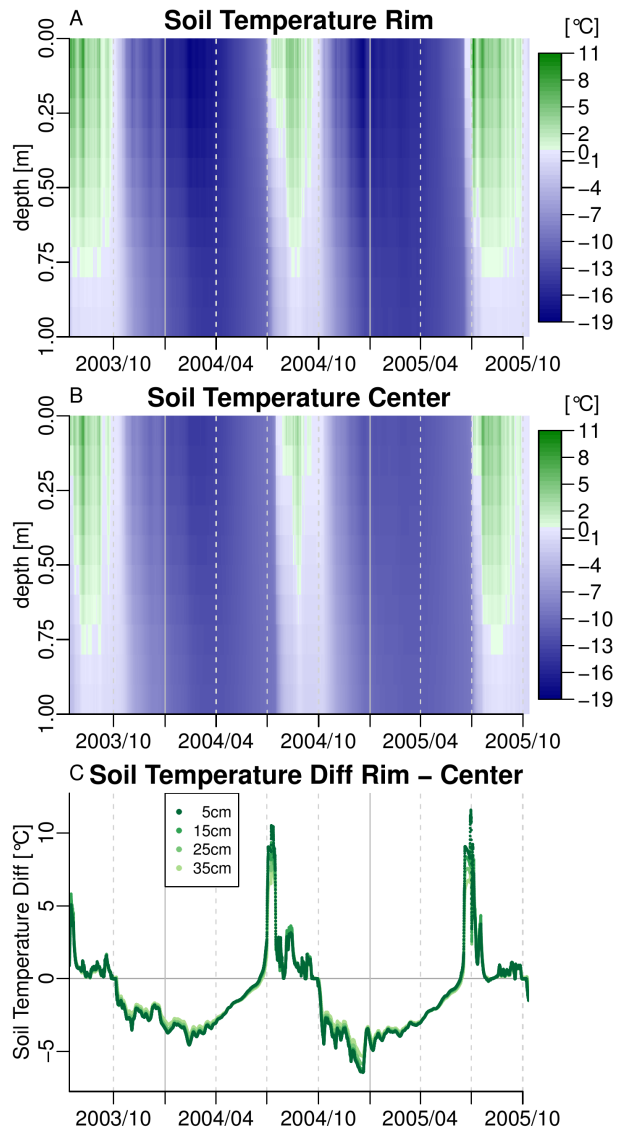


**Figure 10.** Modelled soil temperature of the uppermost metre at (A) rim and (B) center as well as (C) the difference rim minus center in several depths. Solid lines indicate 1st of January, dashed lines indicate 1st of April, 1st of July and 1st of October of the respective year.

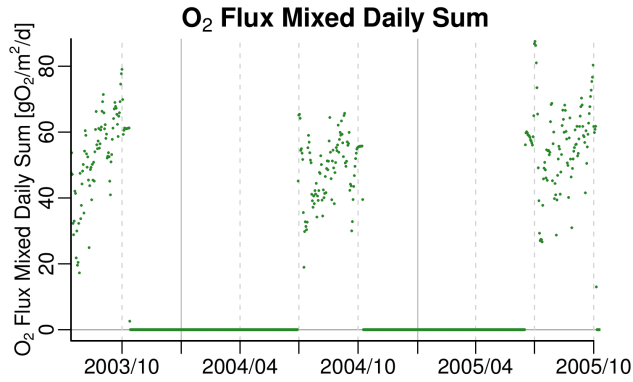


**Figure 11.** Modelled oxygen flux into soil in a mixed approach of 65 % rim plus 35 % center as daily sum. Solid lines indicate 1st of January, dashed lines indicate 1st of April, 1st of July and 1st of October of the respective year. The range of the modelled values is  $-0.00184$  to  $87.6 \text{ gO}_2 \text{ m}^{-2} \text{ d}^{-1}$ .

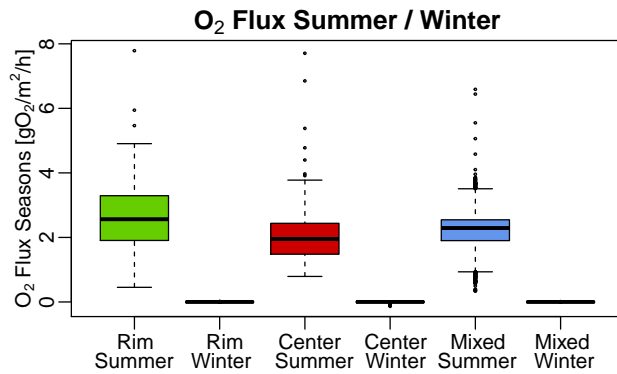


**Figure 12.** Modelled oxygen flux into soil at rim, center and a mixed approach of 65 % rim plus 35 % center, split into summer and winter. Summer means less than 5 cm snow are on the ground, winter is the remainder. Because of the widespread of values, to as high as  $16.3 \text{ gO}_2 \text{ m}^{-2} \text{ h}^{-1}$ , a portion of 0.0118 % values was cut to provide a reasonable picture. The minimum of the values is  $-0.136 \text{ gO}_2 \text{ m}^{-2} \text{ h}^{-1}$ .

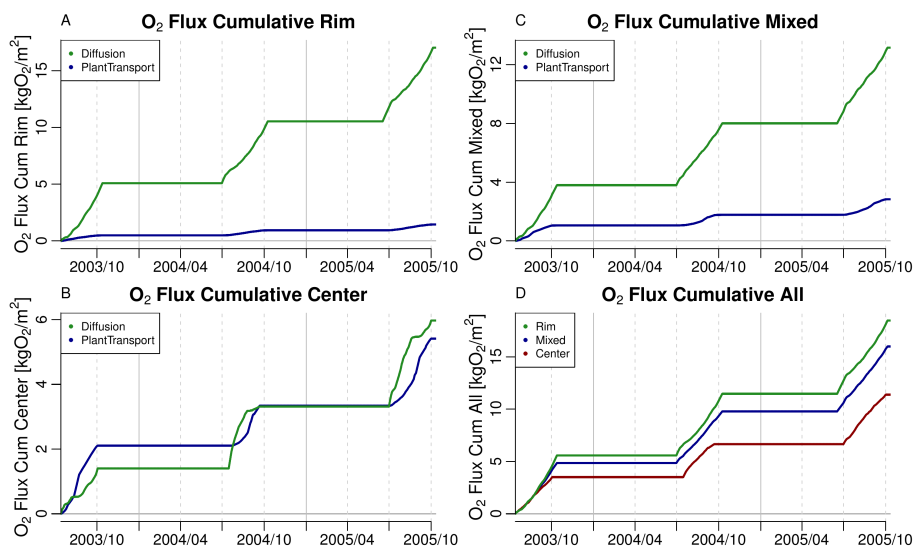


**Figure 13.** Modelled oxygen flux into soil at (A) rim, (B) center, (C) a mixed approach of 65 % rim plus 35 % center, split into the different transport processes, and at (D) rim, center and a mixed approach of 65 % rim plus 35 % center, combined, as cumulative sum. Solid lines indicate 1st of January, dashed lines indicate 1st of April, 1st of July and 1st of October of the respective year. Please note the different scales. Table 5 gives the maximal values.

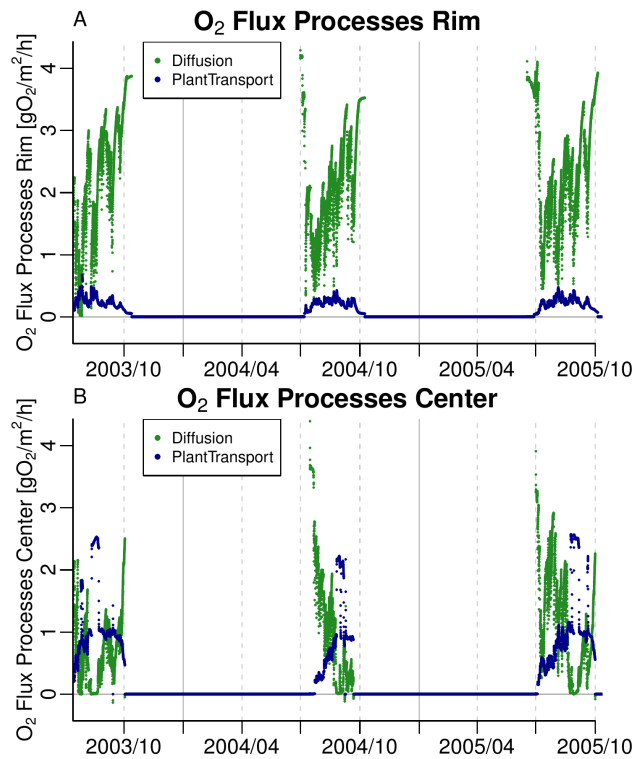


**Figure 14.** Modelled oxygen flux into soil at (A) rim and (B) center, split into the different transport processes. Solid lines indicate 1st of January, dashed lines indicate 1st of April, 1st of July and 1st of October of the respective year. Because of the widespread of high values, to as high as 16.3 (A) and 14.4 (B)  $\text{gO}_2 \text{ m}^{-2} \text{ h}^{-1}$ , a portion of 0.0254 % (A) and 0.0178 % (B) values was cut to provide reasonable pictures. The minima of the values are -0.00185 (A) and -0.136 (B)  $\text{gO}_2 \text{ m}^{-2} \text{ h}^{-1}$ .